STRUCTURAL OPTIMIZATION AND ITS INTERACTION WITH AERODYNAMIC OPTIMIZATION FOR A HIGH SPEED CIVIL TRANSPORT WING

by

Ximing Huang

Dissertation submitted to the Faculty of the
Virginia Polytechnic Institute and State University
in partial fulfillment of the requirements for the degree of

DOCTOR OF PHILOSOPHY

in

Aerospace Engineering

APPROVED:

Dr. R. T. Haftka, Chairman

Dr.B. Grossman

Dr. W. H. Mason

Dr. E. R. Johnson

Dr. R. H. Plaut

September, 1994

Blacksburg, Virginia

STRUCTURAL OPTIMIZATION AND ITS INTERACTION WITH AERODYNAMIC OPTIMIZATION FOR A HIGH SPEED CIVIL TRANSPORT WING

by

Ximing Huang

Committee Chairman: Dr. Raphael T. Haftka

Aerospace Engineering

(ABSTRACT)

A variable-complexity design strategy with combined aerodynamic and structural optimization procedures is presented for the high speed civil transport design (HSCT). Variable-complexity analysis methods are used to reduce the computational expense. A finite element-model based structural optimization procedure with flexible loads is implemented to evaluate the wing bending material weight. Static aeroelastic effects, evaluated through the comparison of rigid and flexible wing models, are found to be small in the HSCT design. The results of structural optimization are compared with two quasi-empirical weight equations. Good correlation is obtained between the structural optimization and one of the weight equations. Based on this comparison, an interlacing procedure is developed to combine both the simple weight equations and structural optimization in the HSCT design optimization, at modest computational cost. HSCT designs based on the interlacing procedure reveal that the aerodynamic optimizer may take advantage of weaknesses in weight equation. However, the optimizer may be unable to escape the local minimum due to the noisy of aerodynamic response and the lack of derivative information for the interlacing procedure.

ACKNOWLEDGEMENTS

I would like to express my heartfelt gratitude to my advisor Prof. R. T. Haftka for his contribution to my academic and professional development. He taught me invaluable lessons in optimization, engineering thinking and sincere altitude to science. As this work has been group effort, I would like to thank Prof. B. Grossman and Prof. W. H. Mason for their most helpful suggestions and comments during the course of this project. I am grateful to my other committee members, Profs. E. R. Johnson and F. H. Lutze for serving on my committee and reading my dissertation. Special thanks go to J. Dudley, M. Hutchison and J. Cruz for their contributions in the areas of aerodynamic and structures. I also wish to acknowledge the assistance I got from Dr. A. McCullers, P. Coen and other fellows in NASA Langley Research Center.

Furthermore, I would like to thank my friends at Virginia Tech, who are too many to name, for always being supportive and kind. I will never forget them.

Finally, I would like to thank my wife Lei. I would not be here without her support and understanding. To her that this work is dedicated.

This work was supported by the NASA Langley Research Center under grant NAG-1-1160 and the National Science Foundation under grant DDM-9008451. The support is gratefully acknowledged.

TABLE OF CONTENTS

LIST OF TABLES

LIST OF FIGURES

1. Introduction

For the last several years, our design group at Virginia Polytechnic Institute and State University has been developing procedures for the design of advanced aircraft by using variable-complexity multidisciplinary optimization methods. As part of this effort, this work is focused on integrating the structural optimization procedure into the aerodynamic optimization procedure for a high speed civil transport optimum design.

1.1 Simultaneous Aerodynamic and Structural Optimization

Advanced aircraft design always involves several disciplines, including aerodynamics, structures, control and propulsion. The balance of the competing requirements of these disciplines, especially the tradeoff between aerodynamic and structural efficiency, is often the major consideration in the design. Aerodynamic designers strive for low-drag slender configurations, but structural weight considerations push in the opposite direction, favoring stubby shapes. The effort to achieve the right balance between conflicting requirements can be traced from bi-plane wing design to modern advanced slender monoplanes.

The interaction of aerodynamics and structures is often inherently of hierarchical nature. The effect of changes in aerodynamic design on structural performance is profound, while the effects of changes in structural design with fixed geometry on aerodynamic performance are usually marginal for transport aircraft. Therefore, aerodynamic design typically precedes structural design. The vehicle designer considers structural requirements at the conceptual design stage and imposes limits on wing airfoil thickness ratios and planform aspect ratios to prevent poor structural

design. However, at the preliminary design stage the aerodynamic design precedes the structural design, and the influence of structural design on the external shape of the wing is ignored. Most of the work on the interaction between aerodynamics and structures has been in the form of aeroelastic effects such as divergence, flutter and loss of control surface effectiveness that introduced the discipline of aeroelasticity. Aeroelastic deficiencies are usually corrected by structural changes, and occasionally structural optimization is used to improve aerodynamic performance, (e.g., Haftka, Ref. 1). The reader interested in work on structural optimization with aeroelastic constraints is referred to Shirk *et al.* (Ref. 2) and Haftka (Ref. 3).

Simple algebraic equations were traditionally used in the conceptual level of aircraft design. These algebraic equations are based on simple analysis models plus a heavy dose of historical data. For example, Malone and Mason (Ref. 4) optimized transport wings in terms of global design variables such as wing areas, aspect ratio, cruise Mach number and cruise altitude using simple algebraic equations for estimating structural and other weights and aerodynamic performance. The same authors also examined the effect of the choice of objective function (maximize range, minimize fuel weight, etc.) using the same equations (Ref. 5). Similarly, Gogate *et al.* (Ref. 6) discussed the effects of cost and economic parameters on the optimum configuration of an air-taxi aircraft by incorporating these parameters into the conceptual equations.

At the preliminary design level, numerical models for both structures and aerodynamics are employed. Early studies of combined aerodynamic and structural optimization relied on simple, usually one dimensional aerodynamic and structural models and a small number of design variables, so that the computational cost was not an important issue. For example, McGeer (Ref. 7) considered the selection of a distribution of lift, chord length and airfoil thickness to minimize induced

drag. Both aerodynamic and structural constraints were evaluated using beam and lifting-line theories. Grossman *et al.* (Ref. 8) demonstrated that simultaneous aerodynamic and structural optimization using such numerical models can produce superior designs to a sequential approach. Wakayama and Kroo (Ref. 9) showed that optimal designs are strongly affected by compressibility drag, aeroelasticity and multiple structural design conditions. Gallman, *et al.* (Ref. 10) have investigated combined aerodynamic-structural optimization for joined-wing aircraft concepts. Recently, Gallman *et al.* (Ref. 11) optimized an advanced business jet using two aircraft optimization codes and identified the errors in the preliminary analysis methods used in the two codes. Today some of these methods, especially for aerodynamic analysis, have migrated into conceptual design tools such as FLOPS (McCullers, Ref. 12), ACSYNT (Vanderplaats, Ref. 13, Mason and Arledge, Ref. 14), PASCOS (Stubbe, Ref. 15) and TRANSYS (Daum and Wolf, Ref. 16).

With the progress of computer hardware and software, more accurate and detailed models, such as the finite element structural analysis, vortex lattice and panel methods which were usually used in the final stage of aircraft design, are moving into the preliminary design level. For example, the coupled aerodynamic, structural and control optimization of a composite forward-swept wing was studied using a finite element model and vortex-lattice aerodynamics by Rais-Rohani (Ref. 17). Using vortex-lattice and supersonic panel aerodynamics, Unger (Ref. 18) optimized a high speed civil transport design. Barthelemy *et al.* (Ref. 19) optimized a high speed civil transport wing structure using an equivalent plate model and taking into consideration static aeroelastic effects. Using a finite element model with 13,700 degrees of freedom and 122 structural design variables, Tzong *et al.* (Ref. 20) optimized the same high speed civil transport configuration. Wakayama and Kroo (Ref. 21) presented some wing planform optimization results for minimum

drag design with constraints on structural weight and maximum lift. Simple beam structural model, vortex method and weight equations were used in this study.

Advanced computational fluid dynamics (CFD) analysis methods are also used in the aerodynamic optimization. For example, Burgreen and Baysal (Ref. 22) demonstrated the three-dimensional aerodynamic shape optimization of supersonic delta wings using a fully implicit Euler equation and discrete sensitivity analysis. Welge (Ref. 23) predicts the benefits obtainable by simultaneous optimization of planform, engine location and structural using three-dimensional Euler and Boundary Layer methods. Some further aerodynamic shape optimization work based on Euler aerodynamic analysis method can be found in Change, *et al.* (Ref. 24) and Korivi *et al.* (Ref. 25).

To address the complex internally coupled problems, Sobieski (Refs. 26, 27, 28) proposed multi-level decomposition approach. The application work based on this approach can be found in Wrenn and Dovi (Ref. 29), Röhl and Schrage (Ref. 30) and Eason *et al.* (Ref. 31). Toward the fully integrated aerodynamic and structural optimization, Kulfan (Ref. 32) investigated a number of unusual configuration concepts for supersonic aircraft, and predicted that significant gains in aerodynamic efficiency may be obtained through the use of design optimization and better design integration procedures. Borland *et al.* (Ref. 33) performed an exploratory study on integrating structural and aerodynamic optimization for commercial aircraft design. Approximate aerodynamic models created based on Navier-Stokes equations were used to evaluate lift, drag and other aerodynamic performances, a small finite element model with a rigid loads was used for structural analysis. Because of computational expense, results after only one optimization cycle were presented to demonstrate the advantage of simultaneous structural and aerodynamic optimization. The computational efficiency becomes an important issue when the complexity

of the aerodynamic and structural models and the number of design variables increase. The high computational cost related to such models typically limits the number of design variables that can be considered.

One of the major components of the computational cost is the calculation of cross-sensitivity derivatives. Those are the derivatives of aerodynamic performance with respect to structural size and derivatives of structural response with respect to changes in aerodynamic shape. Variable-complexity modeling (Refs. 18, 34) seeks to address the expense of interdisciplinary calculations and single-discipline optimization by coupling approximate, conceptual-level models to more advanced, preliminary or detailed-level disciplinary models. This approach offers the benefit of providing greater insight and reduced computational cost while comparing and correcting the performance predicted by simple methods with the more sophisticated techniques. Using this approach, Hutchison *et al.* (Refs. 34, 35) coupled panel methods for aerodynamic performance and simple weight equations for structural weight estimation to optimize a high speed civil transport. However, the simple weight equations are sometimes inaccurate, especially in the estimation of wing structural weight (Refs. 36, 37). A more accurate method has to be implemented to provide the correction for such weight equations (Ref. 38).

1.2 High Speed Civil Transport Design

The particular design problem we are working on is the optimum design of a Mach 2.4 high speed civil transport design which carries 251 passengers and has a range of 5500 n.mi. (see Fig. 1.1). This configuration was developed by the Vehicle Integration Branch at NASA's Langley Research Center as a generic high speed civil transport for technology integration studies. While the design was developed only

as a platform for continuing research, it does reflect current advanced configuration design concepts (Ref. 39).

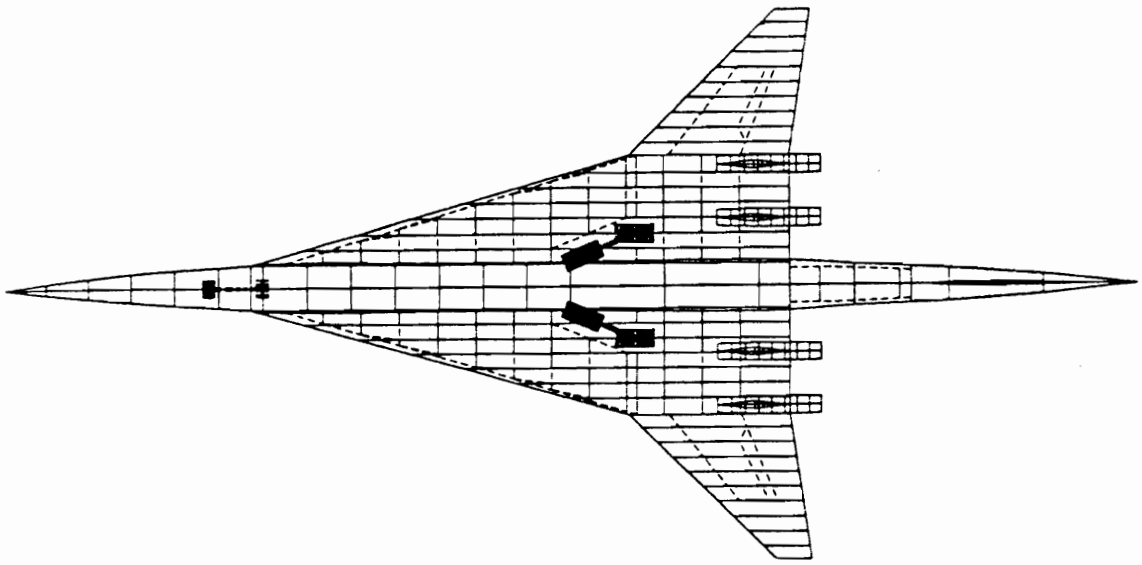

Figure 1.1 Baseline Configuration.

An aerodynamic optimization procedure focusing on improving the fuselage shape, wing planform, airfoil geometry and nacelle locations was implemented to minimize the take-off gross weight design (Ref. 35). Twenty-six design variables are used to describe the complete configuration. The wing planform is described by 8 design variables, and the airfoil thickness distribution with an additional 5. The nacelles move axially with the wing's trailing edge, and 2 parameters define their spanwise locations. The axisymmetric fuselage requires 8 parameters to specify the axial location and radius of the four restraint locations selected to model the baseline configuration and which give us the minimum drag fuselage shape description. While the configuration is defined using this set of parameters, the aircraft geometry

is actually stored as a discrete numerical description in the Craidon format (Ref. 40) and most aerodynamic and structural analysis are performed on this format. In addition to the geometric parameters mentioned above, three variables define the idealized cruise mission. One variable is the mission fuel and the other two specify the initial cruise altitude and the constant climb rate used in the range calculation. There are 53 constraints, including performance/aerodynamic constraints and geometric constraints, which prevent the optimizer from creating physically impossible designs. The variable-complexity modeling approach employed weight equations to predict the effect of changes of structural design on aerodynamic performance in our early multidisciplinary aircraft design method. Because the more detailed aerodynamic calculations, e.g., the Harris program for the wave drag, the supersonic Mach-box type panel method for drag due to lift, or the vortex-lattice program for landing performance, are computationally expensive, a sequential approximate optimization technique was employed in which the overall design process is composed of a sequence of optimization cycles. At the beginning of each cycle, approximations of the wave drag and drag due to lift, based on simpler models, are constructed. These simple models are corrected by scale factors based on the more detailed models which are executed at the beginning of each cycle. Move limits are imposed on the design variables to avoid large errors. There are several methods available for use during the optimization, including linear, scaled, and global-local approximation, all described in Ref. 35. The optimization is performed by the NEWSUMT-A program (Ref. 41), which uses a sequential unconstrained minimization technique and an extended interior penalty function.

An important lesson we learned from the above aerodynamic optimization is that the optimizer may take advantage of weaknesses inherent in simple models.

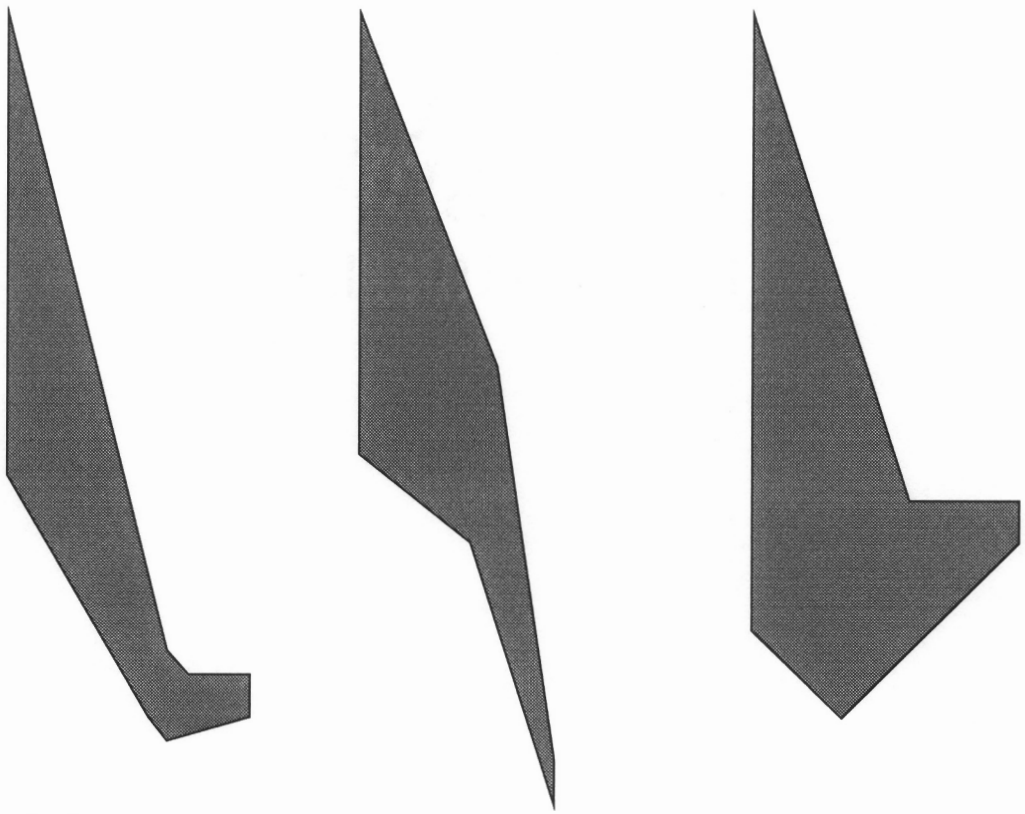

Figure 1.2 Wing Planforms Obtained in Aerodynamic Optimization.

Figure 1.2 shows designs obtained when we used only a simple algebraic approximation for the landing angle of attack. Each of the planforms in the figure corresponds to a different simple model. As can be seen, the aerodynamic optimizer took advantage of the weaknesses of the three simple numerical models and converged to unreasonable designs. When these designs were analyzed by more accurate methods, the required angle of attack was much larger than predicted by the simpler models, even though these models worked well for the baseline configuration. This showed the danger of using simple models and motivated our use of more accurate models for correction of the simple models. This experience raises a similar issue related to the structural modeling used in the aerodynamic optimization. If the

optimizer so successfully took advantage of the weaknesses in the simple landing angle-of-attack models, it may be just as successful take advantage of the weaknesses in the conceptual-level weight estimation methods used in the aerodynamic optimization.

As mentioned before, we have used the statistical weight equations in the Flight Optimization System (FLOPS, Ref. 12) and coupled them to an aerodynamic design procedure for the high speed civil transport. However, since the high speed civil transport is a new aircraft, weight equations may not account for all features of the design. Furthermore, by its nature, a weight equation can provide only a crude estimate of structural weight. A finite-element-model based structural optimization can provide an more accurate estimation of structural weight and its derivatives with respect to aerodynamic design variables. However, this procedure can only predict the load carrying part of the structural weight. Additionally, the procedure is computationally expensive in comparison with statistical weight equations. A full integration of the structural and aerodynamic optimization is very taxing computationally, due to the need for repeated calculation of the aerodynamic loads, and, more importantly, the derivatives of these loads with respect to all the aerodynamic design variables.

1.3 Objective and Outline

The objective of the present work is to achieve a balance between the accuracy and computational expense through performing simultaneous aerodynamic and structural optimization using a variable complexity modeling approach. An interlacing procedure which consists of periodical execution of structural optimization for correction of the weight equation is developed for this purpose. We implemented a finite-element-model based structural optimization to evaluate the wing

bending material weight. Two kinds of external loads were used for the structural optimization: the flexible loads which take account into the coupling between aerodynamic loads and structural deformations and the rigid loads which ignore this coupling effect. The procedure of flexible load evaluation is described in Chapter 2. This procedure is compared with an alternative procedure based on a fixed-point iteration method in the same chapter. The structural optimization procedure, its formulation, modeling, loads and implementation is described in Chapter 3. The magnitude of static aeroelastic effects is evaluated through comparison of optimal designs of some typical wings with rigid and flexible loads. We compare the structural optimization results with the estimates of two weight equations in Chapter 4. A simple interlacing strategy is described in Chapter 4 and three aerodynamic designs are optimized by using this approach.

This work was performed in a team under the guidance of professors Haftka, Grossman and Mason and with collaboration with several other graduate students. I would like to acknowledge the contribution of J. Cruz to the development of the aeroelastic formulation and computer program. Dr. M. Hutchison provided me the vortex-lattice and supersonic panel codes and several aerodynamic designs. J. Dudley and I collaborated on conducting the integrated aerodynamic and structural optimization.

2. Aeroelastic Analysis and Sensitivity

Early structural optimization were performed under fixed loading conditions and neglected the change of aeroelastic loads due to design variable changes. This approach neglects a potential reduction of loads through passive load alleviation. Introduction of aeroelastic load sensitivities to structural design variables and sensitivities of stresses to loads changes in the optimization procedure can lead to true aeroelastic tailoring and hence lighter structural design. Further load reductions and weight savings can also be obtained through active control devices such as spoilers, ailerons, and horizontal tail. The trend in modern aircraft design has been to use simultaneous strength/flutter along with detailed finite element models (Refs. 2, 42). To take into account static aeroelastic effects, we implemented a flexible load generation program. This chapter presents the general analytical formulation of aeroelastic loads and their sensitivity calculation. Trimming for pitch by fuel management is also included in the formulation. In the formulation below, a number of assumptions are made. The aerodynamic loads are assumed to depend only on the vehicle shape, angle of attack, α, flight Mach number, M , and dynamic pressure, q. The elastic deformation of the structure is treated in a quasi-static method. It is assumed that the angle of pitch is small and the forces related to the velocity of pitch angle, $\dot{\theta}$, are negligible. We only consider symmetric cruise and maneuver conditions. The formulation is partly based on J. Cruz's note (Ref. 43) and program, and it is checked against a fixed-point iteration approach.

2.1 Aerodynamic and Gravity Loads

The equation of motion of an aircraft discretized by a finite element model is

$$\mathbf{M}\ddot{\mathbf{u}} + \mathbf{K}\mathbf{u} = \mathbf{F}_a + \mathbf{F}_g + \mathbf{F}_p, \tag{2.1}$$

where $\mathbf{M}$ is the mass matrix, $\mathbf{K}$ is the stiffness matrix, $\mathbf{u}$ is the nodal displacement vector, $\mathbf{F}_a$, $\mathbf{F}_g$ and $\mathbf{F}_p$ represent the applied aerodynamic, gravity and propulsive force vectors, respectively. The vector $\mathbf{u}$ combines both rigid body motion and elastic deformations.

Once the finite element model is set up, the aerodynamic loads are generated using the same codes developed for the aerodynamics optimization. That is, the loads in subsonic flight are calculated from a vortex lattice method (Refs. 44, 45) and the loads in supersonic flight are determined from a supersonic panel method (Ref. 46, 47). The number of panels used in the vortex lattice and supersonic panel methods depends on the geometry and flight Mach number. In the vortex lattice method, a horseshoe vortex is placed in each panel with a control point located at 75% of the chord of the panel as shown in Fig. 2.1.

Using the Biot-Savart law, the relationship between the strength of each vortex filament and the velocity induced by that vortex at a control point over the wing is obtained. Summing the contributions of all horseshoe vortices over both wings, the total induced velocity at each control point is determined. By enforcing flow tangency at the control point of each panel, a vector of circulation strength Γ is computed. The aerodynamic forces are computed from a local application of the Kutta-Joukowsky theorem as

$$\mathbf{F} = \rho \mathbf{V} \times \mathbf{\Gamma}, \tag{2.2}$$

and compressibility effects are included through a Göthert transformation.

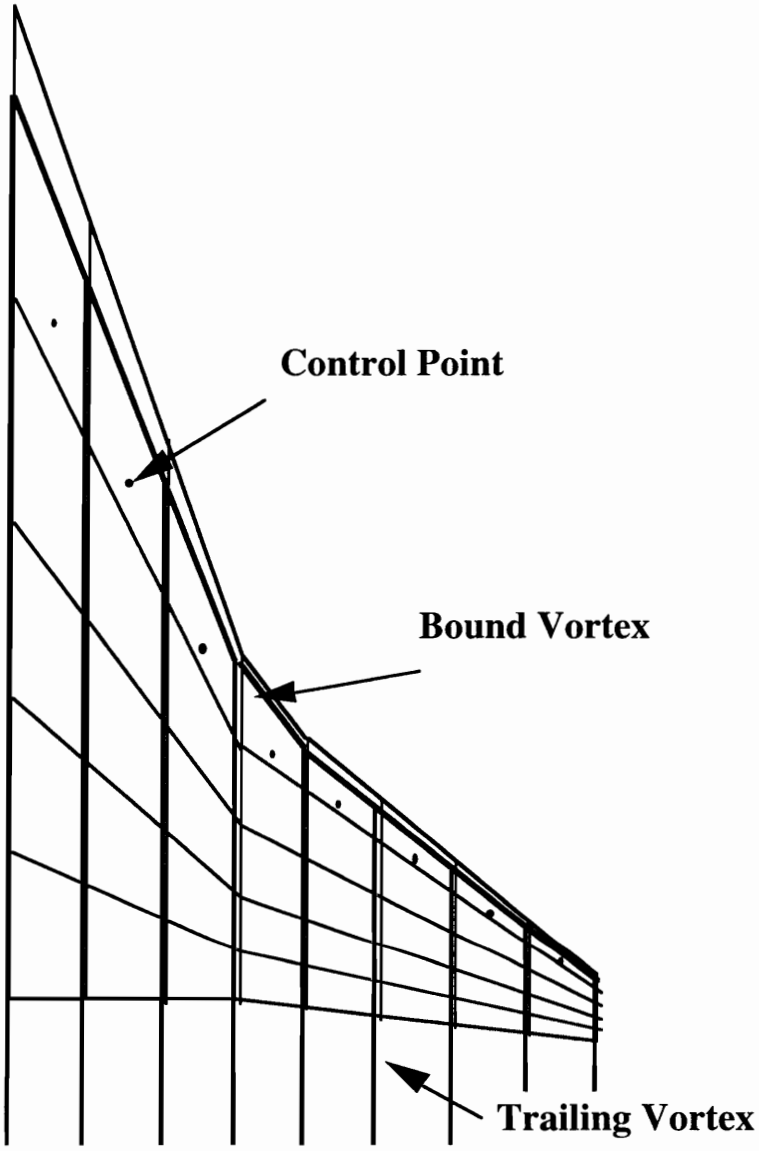

Figure 2.1 Vortex-Lattice Model.

The the supersonic panel method is very similar to the vortex lattice method except that instead of a vortex, a supersonic source and a doublet are placed at the center of each panel. The axis of the doublet is in the positive upward direction and the influences of both the source and the doublet are only present in the zone of

action downstream of the point. The same boundary and Kutta conditions are used to solve for the strengths of these singularities and then the velocity and pressure at each control point.

The structural finite-element nodes usually do not match the location and the number of the aerodynamic control points used in the vortex-lattice and the supersonic panels methods. Hence, it is necessary to develop a mechanism by which the aerodynamic loads are transferred to the structural grid nodes and the structural deformations are transferred to the aerodynamic control points. A surface spline interpolation, developed in Ref. 48, was used to transform the aerodynamic loads and camber slopes to the structural grids and transform the structural displacements and slopes to aerodynamic points.

In the aerodynamic design, we did not specify a wing camber distribution, and assumed that camber could be used to attain the performance required. For structural loads, however, the wing camber and twist make a first order contribution to the aerodynamic load distribution. Thus we used Carlson's WINGDES program (Ref. 46) to generate a wing cambered for optimum cruise, and computed the aerodynamic loads corresponding to this camber at the several selected flight conditions.

We use the FLOPS program to estimate the nonstructural and structural component weights except for the wing bending material weight which is replaced by the most recent structural optimization results. Each nonstructural weight is then redistributed to the finite element nodes in the vicinity of its center of gravity using

$$W_i = (\frac{W}{n})(1 - \frac{D_i - D_{av}}{D_{max} - D_{min}}), \tag{2.3}$$

where

W_i - weight assigned to finite element node i,

W - weight of nonstructural component,

n - number of affected nodes,

D_i - distance from CG of the weight to node i,

D_{av} - average distance from CG of the weight to all affected nodes,

D_{max} - distance from CG of the weight to furthermost node,

D_{min} - distance from CG of the weight to nearest node.

The structural weights are applied to the finite element model directly in the EAL program by adjusting the sizing of elements so that the weight of each structural component equals the estimate of the FLOPS program.

2.2 Aeroelastic Formulation

To reduce the cost of analysis, we use the vibration modes $\mathbf{\Phi}_e$ to approximate the elastic component of the displacement vector, and the displacement vector, $\mathbf{u}$, in equation (2.1) can expressed as

$$\mathbf{u} \cong \mathbf{\Phi}_z u_z + \mathbf{\Phi}_\theta \theta + \mathbf{\Phi}_x u_x + \mathbf{\Phi}_e \mathbf{\Theta}_e, \tag{2.4}$$

where $\mathbf{\Phi}_z$, $\mathbf{\Phi}_\theta$, $\mathbf{\Phi}_x$ and $\mathbf{\Phi}_e$ are the plunge, pitch, fore/aft rigid body modes, and elastic modes, respectively, and u_z, θ, u_x and $\mathbf{\Theta}_e$ are the plunge, pitch, fore/aft rigid body amplitudes, and elastic modal magnitudes, respectively. By using this modal approximation, a system with thousands of degrees of freedom is typically reduced to about twenty or thirty modal coordinates. Here $\mathbf{\Phi}_e$ may represent mode shapes of some nominal structure rather than of the present structure. So $\mathbf{\Phi}_e$ is not necessarily orthonormal with respect to the mass and stiffness matrices. The option of keeping $\mathbf{\Phi}_e$ constant allows us to recalculate the flexible loads without

recalculating the mode shapes when we modify the structure or fuel distribution and this can substantially improve computational efficiency.

For the inertia forces we neglect the acceleration associated with the elastic deformations, that is, treat these in a quasi-static manner, so that

$$\ddot{\mathbf{u}} \cong \mathbf{\Phi_z}\ddot{u}_z + \mathbf{\Phi}_\theta\ddot{\theta} + \mathbf{\Phi_x}\ddot{u}_x \ . \tag{2.5}$$

Substituting back into equation (2.1) we get

$$\mathbf{M\Phi}_z\ddot{u}_z + \mathbf{M\Phi}_\theta\ddot{\theta} + \mathbf{M\Phi}_x\ddot{u}_x + \mathbf{K\Phi}_e\mathbf{\Theta}_e = \mathbf{F}_a + \mathbf{F}_g + \mathbf{F}_p. \tag{2.6}$$

We premultiply equation (2.6) by the transpose of $\mathbf{\Phi}_z$, $\mathbf{\Phi}_\theta$, $\mathbf{\Phi}_x$ and $\mathbf{\Phi}_e$, respectively and to obtain

$$m_{zz}\ddot{u}_z + m_{z\theta}\ddot{\theta} + m_{zx}\ddot{u}_x = f_{az} + f_{gz} + f_{pz}, \tag{2.7}$$

$$m_{z\theta}\ddot{u}_z + m_{\theta\theta}\ddot{\theta} + m_{\theta x}\ddot{u}_x = f_{a\theta} + f_{g\theta} + f_{p\theta}, \tag{2.8}$$

$$m_{zx}\ddot{u}_z + m_{\theta x}\ddot{\theta} + m_{xx}\ddot{u}_x = f_{ax} + f_{px}, \tag{2.9}$$

$$\mathbf{m}_{ze}^T\ddot{u}_z + \mathbf{m}_{\theta e}^T\ddot{\theta} + \mathbf{m}_{xe}^T\ddot{u}_x + \mathbf{k}_{ee}\mathbf{\Theta}_e = \mathbf{f}_{ae} + \mathbf{f}_{ge} + \mathbf{f}_{pe}, \tag{2.10}$$

where the components of generalized mass matrix, stiffness matrix, aerodynamic, gravity and propulsive loads are defined respectively as

$$m_{i,j} = \mathbf{\Phi}_i^T\mathbf{M\Phi}_j,$$

$$\mathbf{m}_{ie}^T = \mathbf{\Phi}_i^T\mathbf{M\Phi}_e,$$

$$\mathbf{k}_{ee} = \mathbf{\Phi}_e^T \mathbf{K} \mathbf{\Phi}_e,$$

$$f_{aj} = \mathbf{\Phi}_j^T \mathbf{F}_a,$$

$$f_{gj} = \mathbf{\Phi}_j^T \mathbf{F}_g,$$

$$f_{pj} = \mathbf{\Phi}_j^T \mathbf{F}_p,$$

$$\mathbf{f}_{ae} = \mathbf{\Phi}_e^T \mathbf{F}_a,$$

$$\mathbf{f}_{ge} = \mathbf{\Phi}_e^T \mathbf{F}_g,$$

$$\mathbf{f}_{pe} = \mathbf{\Phi}_e^T \mathbf{F}_p,$$

and

$$i, j = z, \theta, x.$$

Because of orthogonality,

$$m_{z,x} = m_{xz} = 0,$$

$$\mathbf{\Phi}_z^T \mathbf{K} \mathbf{\Phi}_e = \mathbf{\Phi}_\theta^T \mathbf{K} \mathbf{\Phi}_e = \mathbf{\Phi}_z^T \mathbf{K} \mathbf{\Phi}_e = 0.$$

The generalized propulsive loads, $\mathbf{f}_p$, are assumed to be constant and given, and the generalized aerodynamic load $\mathbf{f}_a$ depends on the wing deformations and angle of attack

$$\mathbf{f}_a = \mathbf{f}_a(\alpha, \mathbf{\Theta}_s), \tag{2.11}$$

where the angle of attack α is related to the pitch angle θ and forward aircraft velocity V as

$$\alpha = \theta - \frac{\dot{u}_z}{V}. \tag{2.12}$$

The elastic shape deformation $\mathbf{\Theta}_s$ is given as

$$\mathbf{\Theta}_s = \mathbf{\Theta}_e + \mathbf{\Theta}_j \ ,$$

where $\mathbf{\Theta}_j$, the jig shape of the wing, is built to correct for elastic deformations in some other flight condition. In this work $\mathbf{\Theta}_j$ is assumed to correct for displacements at middle cruise (load case 1 in table 3.3), so that

$$\mathbf{\Theta}_j = -\mathbf{\Theta}_{ec} \ .$$

We assume that $\mathbf{f}_a$ is approximately linear in its arguments:

$$\mathbf{f}_a \cong \mathbf{f}_{a0} + q\left[\mathbf{A}_\alpha \theta + \mathbf{A}_e(\mathbf{\Theta}_e - \mathbf{\Theta}_{ec})\right] \ , \tag{2.13}$$

where $\mathbf{A}_\alpha$ and $\mathbf{A}_e$ are matrices of derivatives of the aerodynamic loads with respect to α and the elastic deformations, respectively, calculated by finite differences and $\mathbf{f}_{a0}$ is the aerodynamic load vector at an angle of attack of $-\dot{u}_z/V$. With the linear approximation to $\mathbf{f}_a$, equations (2.7) - (2.10) are a set of linear equations

$$m_{zz}\ddot{u}_z + m_{z\theta}\ddot{\theta} = f_{az0} + q(A_{z\alpha}\theta + \mathbf{A}_{ze}(\mathbf{\Theta}_e - \mathbf{\Theta}_{ec})) + f_{gz} + f_{pz}, \tag{2.14}$$

$$m_{z\theta}\ddot{u}_z + m_{\theta\theta}\ddot{\theta} + m_{\theta x}\ddot{u}_x = f_{a\theta 0} + q(A_{\theta\alpha}\theta + \mathbf{A}_{\theta e}(\mathbf{\Theta}_e - \mathbf{\Theta}_{ec})) + f_{g\theta} + f_{p\theta}, \tag{2.15}$$

$$m_{\theta x}\ddot{\theta} + m_{xx}\ddot{u}_x = f_{ax0} + q(A_{x\alpha}\theta + \mathbf{A}_{xe}(\mathbf{\Theta}_e - \mathbf{\Theta}_{ec})) + f_{px}, \tag{2.16}$$

$$\mathbf{m}_{ze}^T\ddot{u}_z + \mathbf{m}_{\theta e}^T\ddot{\theta} + \mathbf{m}_{xe}^T\ddot{u}_x + \mathbf{k}_{ee}\mathbf{\Theta}_e = \mathbf{f}_{ae0} + q(\mathbf{A}_{e\alpha}\theta + \mathbf{A}_{ee}(\mathbf{\Theta}_e - \mathbf{\Theta}_{ec})) + \mathbf{f}_{ge} + \mathbf{f}_{pe}. \tag{2.17}$$

The gravity load $\mathbf{f}_g$ is equal to the inertial load produced by $\ddot{u}_z = g$. With the actual $\ddot{u}_z = -(n-1)g$ we have

$$m_{zz}\ddot{u}_z = -(n-1)f_{gz} \ , \tag{2.18}$$

$$m_{z\theta}\ddot{u}_z = -(n-1)f_{g\theta}, \tag{2.19}$$

$$\mathbf{m}_{ze}^T\ddot{u}_z = -(n-1)\mathbf{f}_{ge}. \tag{2.20}$$

We combine the inertial and gravity components and rewrite equations (2.14)-(2.17) as

$$m_{z\theta}\ddot{\theta} = f_{az0} + q(A_{z\alpha}\theta + \mathbf{A}_{ze}(\mathbf{\Theta}_e - \mathbf{\Theta}_{ec})) + nf_{gz} + f_{pz}, \tag{2.21}$$

$$m_{\theta\theta}\ddot{\theta} + m_{\theta x}\ddot{u}_x = f_{a\theta 0} + q(A_{\theta\alpha}\theta + \mathbf{A}_{\theta e}(\mathbf{\Theta}_e - \mathbf{\Theta}_{ec})) + nf_{g\theta} + f_{p\theta}, \tag{2.22}$$

$$m_{\theta x}\ddot{\theta} + m_{xx}\ddot{u}_x = f_{ax0} + q(A_{x\alpha}\theta + \mathbf{A}_{xe}(\mathbf{\Theta}_e - \mathbf{\Theta}_{ec})) + f_{px}, \tag{2.23}$$

$$\mathbf{m}_{\theta e}^T\ddot{\theta} + \mathbf{m}_{xe}^T\ddot{u}_x + \mathbf{k}_{ee}\mathbf{\Theta}_e = \mathbf{f}_{ae0} + q(\mathbf{A}_{e\alpha}\theta + \mathbf{A}_{ee}(\mathbf{\Theta}_e - \mathbf{\Theta}_{ec})) + n\mathbf{f}_{ge} + \mathbf{f}_{pe}. \tag{2.24}$$

Equations (2.21)-(2.24) are a set of linear algebraic equations for $\ddot{\theta}$,θ,$\ddot{u}_x$ and $\mathbf{\Theta}_e$ at a given time and they are solved using LU decomposition (Ref. 49) after we get the solution of the jig shape, $\mathbf{\Theta}_{ec}$, under mid-cruise condition.

Because the above modal solution is not accurate enough to calculate the structural displacements and stresses, the detailed finite element model is still used for the static analysis and sensitivity calculation. In this approach the modal aeroelastic deflections are first used to calculate the rigid accelerations and approximate elastic deformations. Then the generalized inertial and aeroelastic loads are transformed to the finite element nodes using

$$\mathbf{F}_I \cong \mathbf{M}(-\mathbf{\Phi}_\theta \ddot{\theta} - \mathbf{\Phi}_x \ddot{u}_x - n\mathbf{\Phi}_z g), \tag{2.25}$$

$$\mathbf{F}_a \cong \mathbf{M_0}\mathbf{\Phi}[\mathbf{f}_{a0} + q\mathbf{A}_\alpha \theta + \mathbf{A}_e(\mathbf{\Theta}_e - \mathbf{\Theta}_{ec})], \tag{2.26}$$

where $\mathbf{M_0}$ is the mass matrix corresponding to $\mathbf{\Phi}$. These inertial and aerodynamic loads are fully balanced. The external loads are then used in a direct static finite element analysis (rather than a modal solution) for accurate stress and internal loads analysis. Similarly, we can calculate the sensitivities of inertial and aerodynamic loads in the structural system by the same way.

2.3 Fuel Management

The high speed civil transport configurations we are considering at this stage has no horizontal tail, and we assume that the longitudinal trim of the aircraft is accomplished by moving fuel among the various fuel tanks. For the cruise conditions this requires a fuel management procedure to balance the aircraft in straight and level, steady flight at a given Mach number and dynamic pressure.

We assume that cruise elastic deformations are corrected through the jig shape for an average cruise condition. Neglecting variations in structural deformations during cruise, the aerodynamic load, $\mathbf{f}_a$, is assumed to be a linear function of θ and does not depend on the wing deformations. The gravity load $\mathbf{f}_g$ may be written as

$$\mathbf{f}_g = \mathbf{f}_{g0} + \sum_{i=1}^{n_t} (W_i - W_{i0}) \mathbf{f}_{gi}, \tag{2.27}$$

where $\mathbf{f}_{g0}$ is the load corresponding to a nominal set of fuel weights W_{i0} in n_t fuel tanks, $\mathbf{f}_{gi}$ is the gravity load due to a unit weight in the ith fuel tank, and W_i is the actual weight of fuel in the ith tank. For cruise $n = 1$ and $\ddot{\theta} = \ddot{u_z} = 0$, Equations (2.21) - (2.24) may be simplified as

$$f_{az0} + qA_{z\alpha}\theta + f_{gz} + f_{pz} = 0, \tag{2.28}$$

$$f_{a\theta 0} + qA_{\theta\alpha}\theta + f_{g\theta} + f_{p\theta} = 0, \tag{2.29}$$

$$f_{ax0} + qA_{x\alpha}\theta + f_{px} = 0, \tag{2.30}$$

$$\mathbf{k}_{ee}\mathbf{\Theta}_{ec} = \mathbf{f}_{ae0} + q\mathbf{A}_{e\alpha}\theta + \mathbf{f}_{ge} + \mathbf{f}_{pe}. \tag{2.31}$$

Equation (2.30) defines the thrust requirement. We neglect in this work the effect of structural weight change on this requirement, and so we can ignore this equation. Equation (2.28) defines the lift requirement and is used to calculate the required θ (hence angle of attack). Equation (2.29) is the pitch equilibrium equation and constitutes a constraint on the fuel weight distribution. Since there are many ways to distribute the fuel, we define an optimization problem that seeks the fuel distribution closest to the nominal one:

Minimize :

$$\sum_{i=1}^{n_t} (W_i - W_{i0})^2$$

Subject to :

$$\sum_{i=1}^{n_t}(W_i - W_{i0}) = 0,$$

$$f_{a\theta 0} + qA_{\theta\alpha}\theta + f_{g\theta} + f_{p\theta} = 0,$$

$$0 \leq W_i \leq W_i^{max}.$$

After this optimization is performed using nonlinear program NEWSUMT-A, equation (2.31) is used to calculate the cruise structural deformations.

2.4 Sensitivity Calculation

For convenience we discuss sensitivity derivatives with respect to a single structural parameter s. The process of derivative calculation begins with the cruise condition. To avoid the need for solving the fuel optimization problem every time we change the structure, and to simplify derivative calculation, we assume that we move fuel only between the foremost and rearmost available tanks. For this case, equation (2.27) may be written as

$$\mathbf{f}_g = \mathbf{f}_{g0} + \triangle W_f \mathbf{f}_{gf}, \tag{2.32}$$

where $\triangle W_f$ is the amount of fuel moving aft and $\mathbf{f}_{gf}$ is the change in $\mathbf{f}_g$ for unit $\triangle W_f$. In this case, the fuel management optimization problem reduces to solving the pitch equilibrium constraint equation for $\triangle W_f$:

$$f_{a\theta 0} + qA_{\theta\alpha}\theta + f_{p\theta} + f_{g\theta 0} + \triangle W_f f_{g\theta f} = 0. \tag{2.33}$$

To start the sensitivity calculation we differentiate equations (2.28) and (2.33) with respect to the structural design variable s:

$$qA_{z\alpha}\frac{d\theta}{ds} + \frac{df_{gz0}}{ds} + \frac{d\triangle W_f}{ds}f_{gzf} = 0, \tag{2.34}$$

$$qA_{\theta\alpha}\frac{d\theta}{ds} + \frac{df_{g\theta 0}}{ds} + \frac{d\triangle W_f}{ds}f_{g\theta f} = 0. \tag{2.35}$$

We can solve equations (2.34) and (2.35) for $\frac{d\theta}{ds}$ and $\frac{d\triangle W_f}{ds}$. Next we differentiate equation (2.31) to get

$$\mathbf{k}_{ee}\frac{d\mathbf{\Theta_{ec}}}{ds} = q\mathbf{A}_{e\alpha}\frac{d\theta}{ds} + \frac{d\mathbf{f}_{ge0}}{ds} + \frac{d\triangle W_f}{ds}\mathbf{f}_{gef} - \frac{d\mathbf{k}_{ee}}{ds}\mathbf{\Theta}_{ec}, \tag{2.36}$$

from which we can calculate the derivative of the cruise displacement vector $\mathbf{\Theta}_{ec}$. Then we differentiate equations (2.13), (2.21) - (2.24) to get

$$\frac{d\mathbf{f}_a}{ds} = q\mathbf{A}_\alpha\frac{d\theta}{ds} + q\mathbf{A}_e(\frac{d\mathbf{\Theta}_e}{ds} - \frac{d\mathbf{\Theta}_{ec}}{ds}). \tag{2.37}$$

$$m_{z\theta}\frac{d\ddot{\theta}}{ds} - qA_{z\alpha}\frac{d\theta}{ds} - q\mathbf{A}_{ze}\frac{d\mathbf{\Theta}_e}{ds} = -\frac{dm_{z\theta}}{ds}\ddot{\theta} + n\frac{df_{gz}}{ds} - q\mathbf{A}_{ze}\frac{d\mathbf{\Theta}_{ec}}{ds}, \tag{2.38}$$

$$m_{\theta\theta}\frac{d\ddot{\theta}}{ds} + m_{\theta x}\frac{d\ddot{u}_x}{ds} - qA_{\theta\alpha}\frac{d\theta}{ds} - q\mathbf{A}_{\theta e}\frac{d\mathbf{\Theta}_e}{ds} = -\frac{dm_{\theta\theta}}{ds}\ddot{\theta} - \frac{dm_{\theta x}}{ds}\ddot{u}_x + n\frac{df_{g\theta}}{ds} - q\mathbf{A}_{\theta e}\frac{d\mathbf{\Theta}_{ec}}{ds},$$

(2.39)

$$m_{\theta x}\frac{d\ddot{\theta}}{ds} + m_{xx}\frac{d\ddot{u}_x}{ds} - qA_{x\alpha}\frac{d\theta}{ds} - q\mathbf{A}_{xe}\frac{d\mathbf{\Theta}_e}{ds} = -\frac{dm_{\theta x}}{ds}\ddot{\theta} - \frac{dm_{xx}}{ds}\ddot{u}_x - q\mathbf{A}_{xe}\frac{d\mathbf{\Theta}_{ec}}{ds}, \tag{2.40}$$

$$\mathbf{m}_{\theta e}^T \frac{d\ddot{\theta}}{ds} + \mathbf{m}_{xe}^T \frac{d\ddot{u}_x}{ds} - q\mathbf{A}_{e\alpha}\frac{d\theta}{ds} - (q\mathbf{A}_{ee} - \mathbf{k}_{ee})\frac{d\mathbf{\Theta}_e}{ds} = -\frac{d\mathbf{m}_{\theta e}^T}{ds}\ddot{\theta} - \frac{d\mathbf{m}_{xe}^T}{ds}\ddot{u}_x + n\frac{d\mathbf{f}_{ge}}{ds}$$

$$-q\mathbf{A}_{ee}\tfrac{d\mathbf{\Theta}_{ec}}{ds} - \tfrac{d\mathbf{k}_{ee}}{ds}(\mathbf{\Theta}_e - \mathbf{\Theta}_{ec}). \quad (2.41)$$

In equations (2.38) - (2.41), $\frac{d\mathbf{f}_a}{ds}$ is substituted from equation (2.37) , and $\frac{d\mathbf{f}_g}{ds}$ and $\frac{d\mathbf{m}_g}{ds}$ have a structural component plus a fuel component obtained by solving equations (2.34) - (2.35). Equations (2.38) - (2.41) are very similar to equations (2.21) - (2.24) and can be solved directly.

2.5 Fixed-Point Iteration Approach

To check and confirm the formulation in the last section, we also implemented a fixed-point iteration procedure to generate the aerodynamic loads under the same assumptions as before. To solve the equation (2.1) by using the fixed point iteration method, the exact displacements may be expressed as

$$\mathbf{u} = u_z\mathbf{\Phi_z} + \theta\mathbf{\Phi}_\theta + u_x\mathbf{\Phi}_x + \mathbf{u_e}, \quad (2.42)$$

and similarly

$$\ddot{\mathbf{u}} \cong \ddot{u}_z\mathbf{\Phi}_z + \ddot{\theta}\mathbf{\Phi}_\theta + \ddot{u}_x\mathbf{\Phi}_x. \quad (2.43)$$

Substituting equations (2.42) and (2.43) back into equation (2.1) we have

$$\mathbf{M\Phi}_z\ddot{u}_z + \mathbf{M\Phi}_\theta\ddot{\theta} + \mathbf{M\Phi}_x\ddot{u}_x + \mathbf{Ku}_e = \mathbf{F}_a + \mathbf{F}_g + \mathbf{F}_p. \quad (2.44)$$

Note that $\mathbf{M\Phi}_z = \frac{1}{g}\mathbf{F}_g$ and $\ddot{u}_z = (n-1)g$ where n is the load factor, so that

$$\mathbf{M}\mathbf{\Phi}_z\ddot{u}_z = -(n-1)\mathbf{F}_g. \tag{2.45}$$

Equation (2.44) may be rewritten in an iterative format as

$$\mathbf{K}\mathbf{u}_{e_i} = \mathbf{F}_{a_{i-1}} + n\mathbf{F}_g + \mathbf{F}_p - \mathbf{M}\mathbf{\Phi}_\theta\ddot{\theta} - \mathbf{M}\mathbf{\Phi}_x\ddot{u}_x \ . \tag{2.46}$$

To calculate $\mathbf{u}_{e_i}$, we need to determine $\ddot{\theta}$, θ and $\ddot{u}_x$ at first. This can be done in a similar way as before. Premultiplying equation (2.44) by $\mathbf{\Phi}_z$, $\mathbf{\Phi}_\theta$ and $\mathbf{\Phi}_x$ we get equations (2.7) - (2.9). For a given shape,

$$\mathbf{F}_a \cong \mathbf{F}_{a0} + q\mathbf{A}_\alpha\theta. \tag{2.47}$$

Substituting equations (2.45) and (2.47) into equations (2.7) - (2.9) , we get

$$m_{z\theta}\ddot{\theta} - qA_{z\alpha}\theta = f_{az0} + nf_{gz} + f_{pz}, \tag{2.48}$$

$$m_{\theta\theta}\ddot{\theta} + m_{\theta x}\ddot{u}_x - qA_{\theta\alpha}\theta = f_{a\theta 0} + nf_{g\theta} + f_{p\theta}, \tag{2.49}$$

$$m_{\theta x}\ddot{\theta} + m_{xx}\ddot{u}_x - qA_{x\alpha}\theta = f_{ax0} + f_{px}. \tag{2.50}$$

In cruise conditions ($\ddot{\theta} = 0$, $\ddot{u}_x = 0$), equation (2.48) is used to calculate θ, equation (2.49) constitutes a constraint on the fuel distribution and a similar optimization procedure is used to seek the fuel distribution closest to the nominal one, and equation (2.46) is used to calculate $\mathbf{u}_{ec}$. In maneuver conditions, the three linear equations (2.47) - (2.50) are used to calculate $\ddot{\theta}$, θ and $\ddot{u}_x$, equation (2.46) is used to calculate $\mathbf{u}_e$.

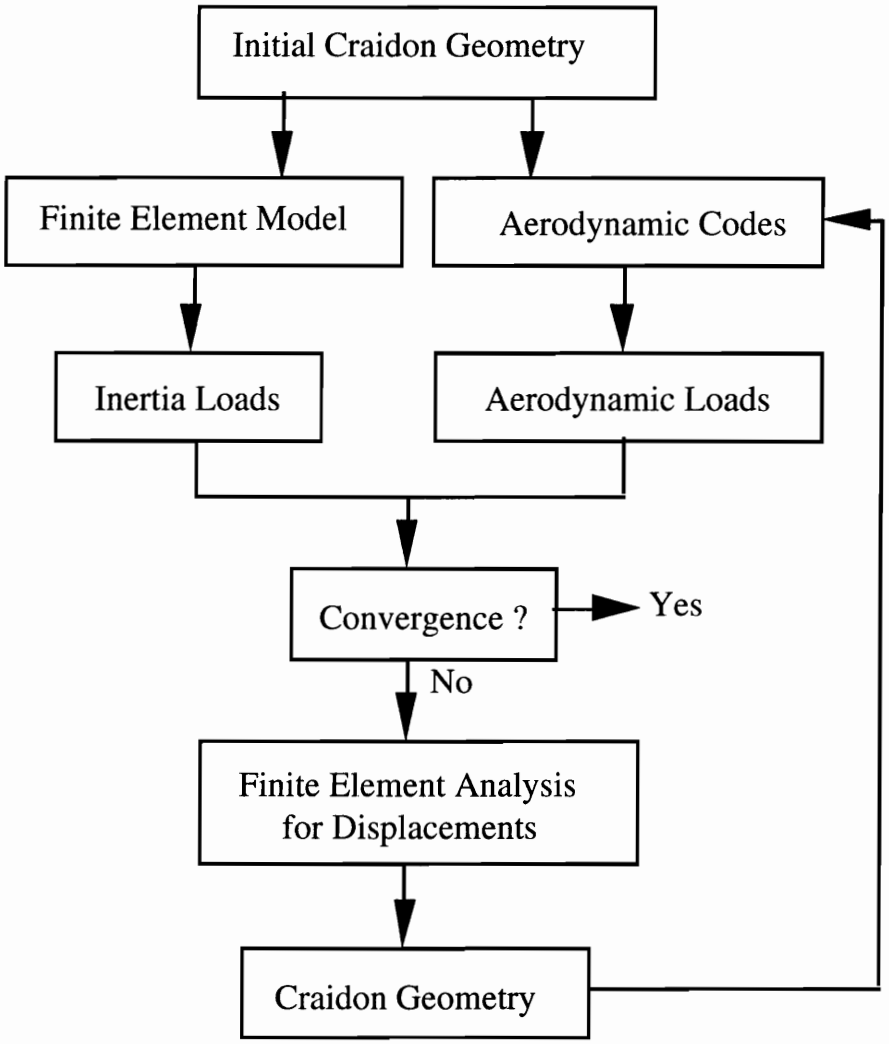

Figure 2.2 Procedure of Fixed-Point Iteration Approach.

The implementation of this procedure is described in Fig. 2.2. Starting from the rigid finite element model and rigid loads, we can solve equations (2.47) - (2.50) to get the rigid acceleration and then update the inertia loads. The singularity of the stiffness matrix in equation (2.46) can be eliminated by introducing supports, and this equation is then used to solve for the elastic deformations and update the Craidon geometry. New aerodynamic loads are then generated from the updated Craidon geometry. This procedure is iterated until convergent aerodynamic and

inertia loads are obtained. The sensitivities are calculated by the finite difference method using the same procedure.

2.6 Validation

We applied both methods described above to the M2.4 baseline design for several flight conditions. Table 2.1 compares the the aerodynamic centers of pressure calculated from both methods, where X is the percent location of the aerodynamic center along the fuselage axis, and Y is the percent location of the aerodynamic center along the spanwise direction. 20 modes were used for the first four flight conditions, and 30 modes were used for the last flight condition because the transonic flight condition needs more modes to converge. As can be seen, a good agreement was obtained between the two methods. The modal reduction method, however, is much cheaper than the fixed-point iteration for repeated analysis. This is due to the need to calculate aerodynamic loads only once for the shape corresponding to the vibration modes of the initial structure. The computational time on IBM RISC 6000 used to genarate the flexible loads of five load conditions for a finite element model with 597 degrees of freedom and 40 design variables by modal reduction method and that of fixed-point iteration method are compared in Table 2.2. The modal reduction method requires an initial CPU time used for the normal mode analysis and the calculation of aeroelastic coefficients. The time for each optimization cycle includes the CPU time used to generate the flexible loads and their derivatives with respect to 40 design variables during each structural optimization cycle. The computational time of modal method is almost independent to the number of optimization cycles; while the computational time used in fixed-point iteration method depends on the number of design variables and optimization cycles. With

large number of optimization cycles, we can substantially reduce the computational expense by using the modal reduction method.

Table 2.1 Comparison of Aerodynamic Pressure Center Between Fixed-Point Iteration and Modal Reduction.

Load Case	Mach Number	Load Factor	Fixed Point Iteration		Modal Reduction	
			X	Y	X	Y
1	0.6	1.5	0.556947	0.420102	0.556940	0.420057
2	0.6	2.5	0.556933	0.419297	0.556920	0.419244
3	2.4	1.5	0.533193	0.374145	0.533144	0.374543
4	2.4	2.5	0.534146	0.369467	0.534371	0.366507
5	1.2	2.5	0.561589	0.426228	0.559324	0.432662

Table 2.2. CPU Time (sec) for Flexible Load Generation on IBM RISC 6000.

	Modal Reduction Method	Fixed-Point Iteration Method
Initial	929.1	0
Each Cycle	21.4	731.7

3. Structural Optimization

A finite-element-model based structural optimization procedure was implemented to evaluate the load carrying structural weight. The aeroelastic effects were included using the flexible load generation approach described in the last chapter. This procedure was performed with a fixed wing, fuselage and nacelle configuration for titanium wing skin by using a finite-element model in EAL program (Ref. 50). The optimization was performed using sequential linear programming with a typical starting move limit of 20%.

3.1 Formulation of Structural Optimization

The weight obtained from a finite element model is quite inadequate in itself for predicting the weight of a complex wing structure. It does not account for items such as rivets, joints and local reinforcements. Therefore, we have chosen wing-skin-material weight as the objective function. To ensure that the weight taken from the finite element model is only that used to support bending loads, we subtract from the total the weight used in the control surface regions of the wing and that of the panels at minimum gage thickness.

As discussed in a later section, the initial set of design variables that we chose for the structural optimization was not entirely adequate for the problem, and a second, more refined set was developed. We refer to the two sets as the initial and refined design variable sets, respectively.

Within each set, the variables may be grouped into two categories: those that define the wing panel thicknesses, and those that define spar and rib cap areas. In the initial set, there was a total of 30 design variables: 18 for panel thicknesses,

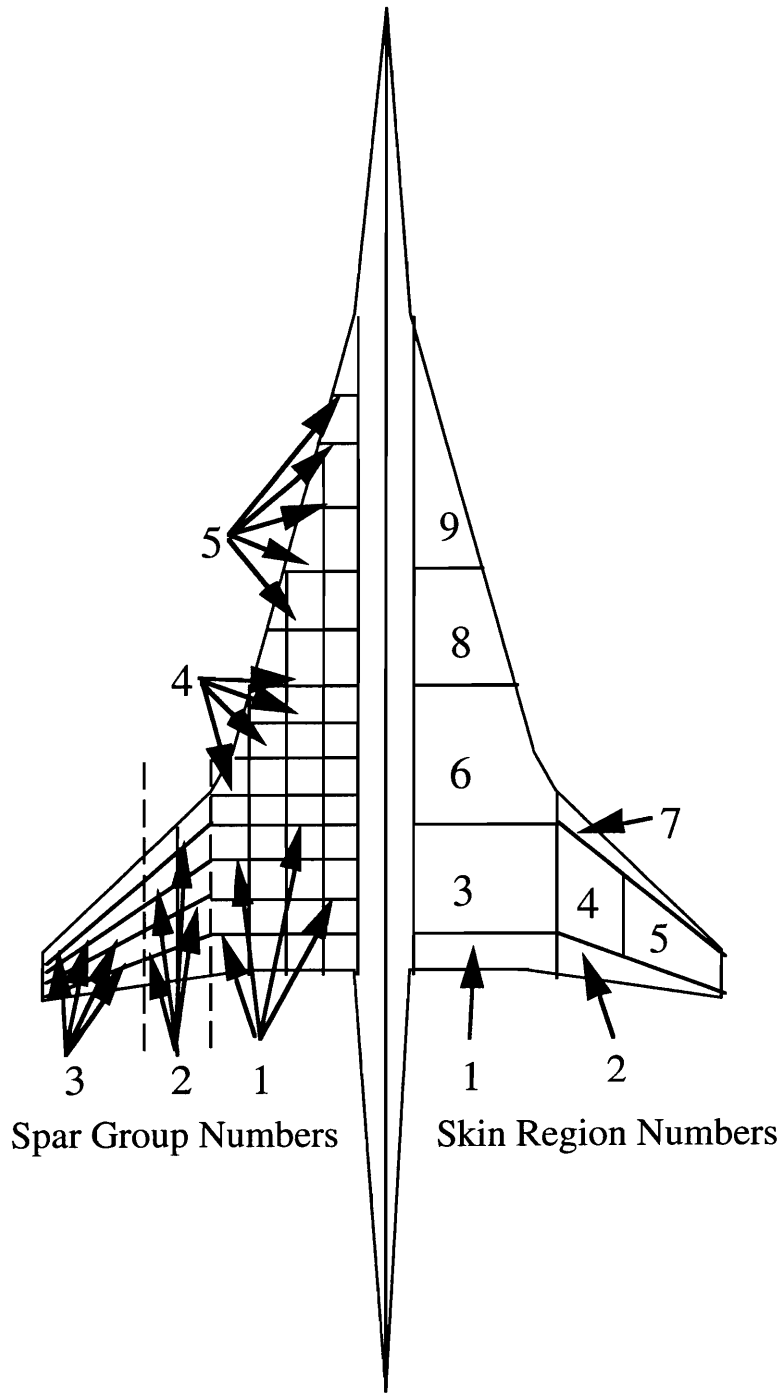

Figure 3.1 Initial Structural Design Variables.

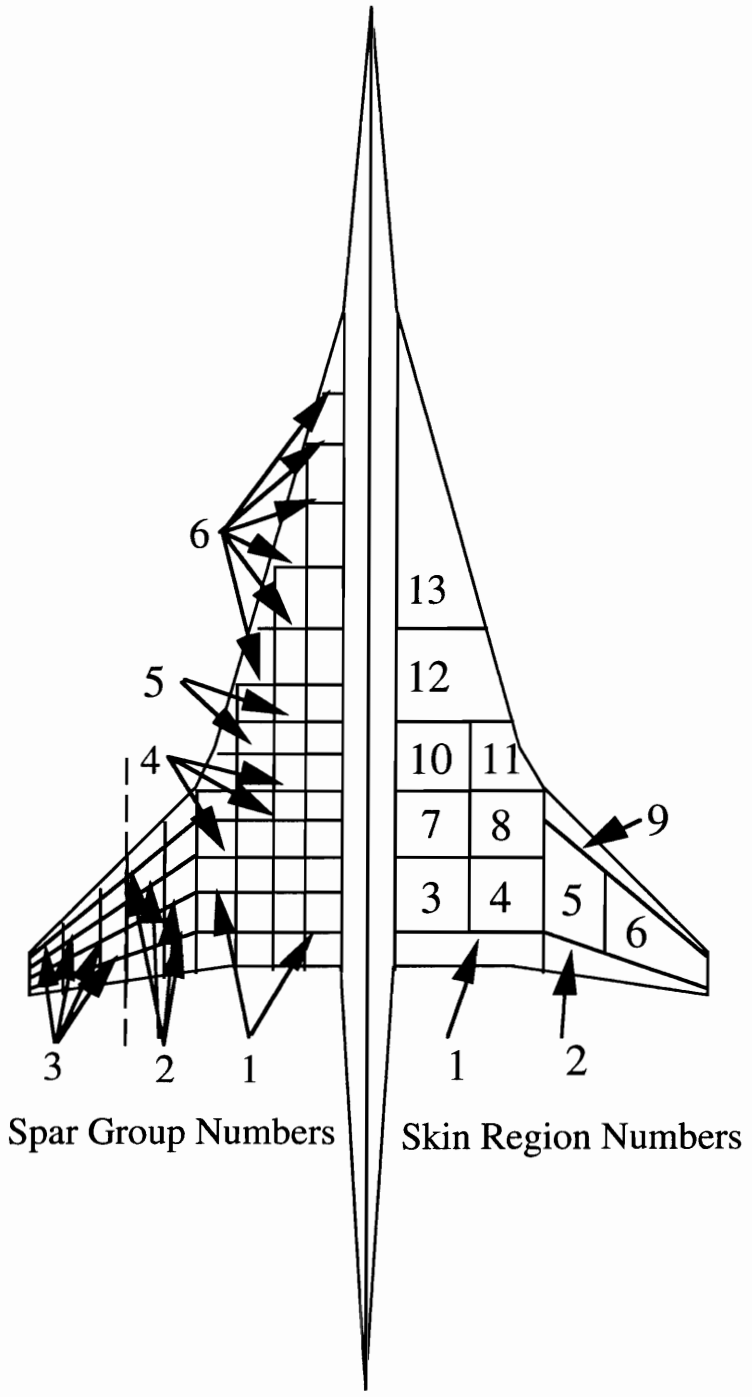

Figure 3.2 Refined Structural Design Variables.

10 for spar cap areas and 2 for rib cap areas. Figure 3.1 illustrates these design variables. The wing skin is divided into 9 regions with each region having two design

variables: one each for the skin thickness on the top and the bottom of the wing. The spars are divided into five groups, with the cap areas of each group on the top and bottom of the wing defined by two design variables. Finally, the rib cap areas are defined with two variables, one for the areas on the top and one for the bottom of the wing.

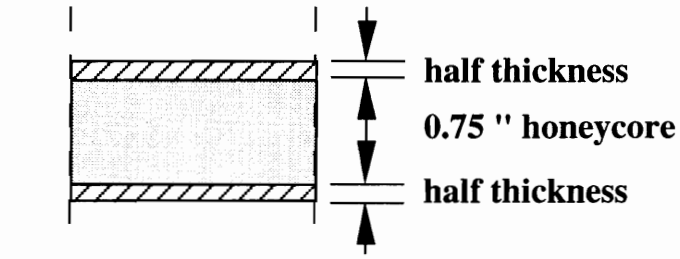

Section of Wing Skin
(Titanium Sandwich Panel)

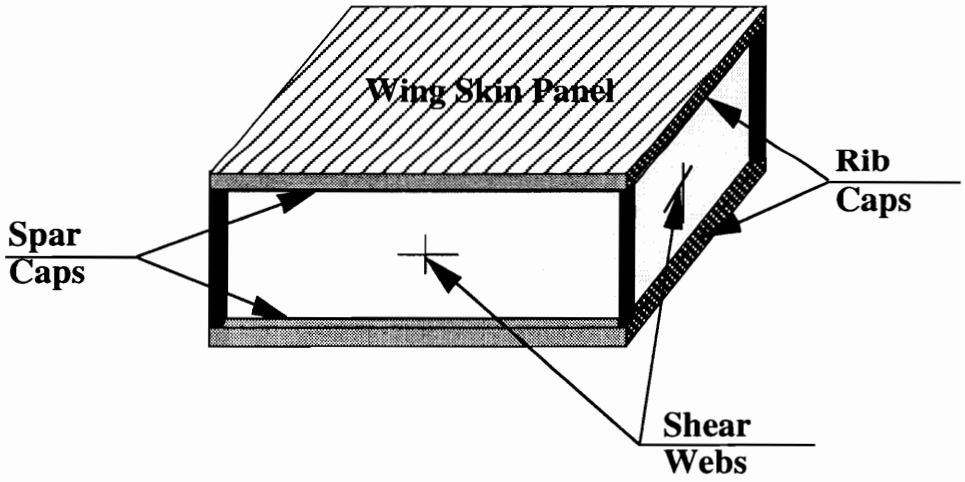

Figure 3.3 Close-up View of Wing Box Cell.

In the refined structural design variable set, we use 40 design variables: 26 to define the skin panel thicknesses, 12 for the spar cap areas; and only two design

variables: one each for the skin thickness on the top and the bottom of the wing. The spars are divided into five groups, with the cap areas of each group on the top and bottom of the wing defined by two design variables. Finally, the rib cap areas are defined with two variables, one for the areas on the top and one for the bottom of the wing.

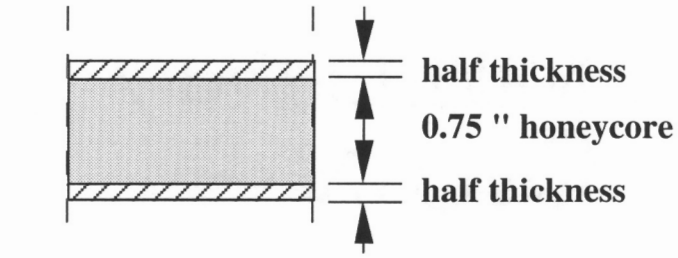

Section of Wing Skin
(Titanium Sandwich Panel)

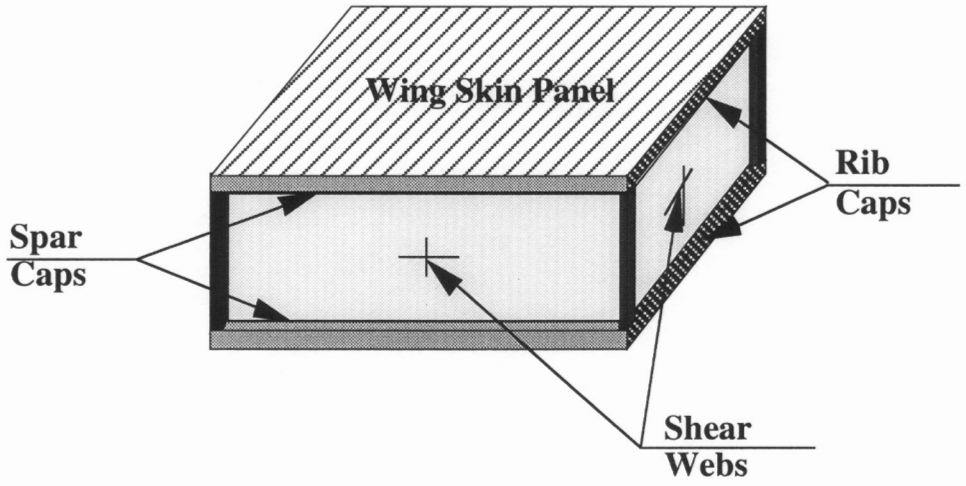

Figure 3.3 Close-up View of Wing Box Cell.

In the refined structural design variable set, we use 40 design variables: 26 to define the skin panel thicknesses, 12 for the spar cap areas; and only two design

where R_{FG} means correlation coefficient between FLOPS and Grumman weight equations, etc. The three factors indicate that the FLOPS weight equation agrees with the structural optimization results much better than the Grumman weight equation as to the effect of geometry changes on the weight.

Because some of the differences between the predictions may be caused by the airfoil thickness distribution rather than the planform shape, we checked the effects of airfoil thickness by optimizing the planform of design 6 in Fig. 4.1 with thicknesses increased and decreased by 10%. As we can see from Table 4.1, the FLOPS weight equation and the structural optimization predict similar effects due to the change of airfoil thickness.

Table 4.1. Effects of Wing Thickness on Predicted Bending Material Weight (lbs) of Design 6 in Fig. 4.1

	-10% Thickness	Original	+10% Thickness
FLOPS	32192	28810	26232
Structural	44728	40924	36449
Ratio	1.389	1.421	1.390

Our comparison shows that the estimates of both weight equations agree well on average with weights predicted by structural optimization. These weight equations can capture most features of advanced aircraft design, but have difficulty to capture the effects of geometry change on structural weight, especially for unconventional designs. For example, FLOPS did not capture the difficulty of having a very thin and elongated outer wing for design 7, leading to a 50 % discrepancy. The aerodynamic optimization using only FLOPS can obtain unrealistic designs unless the weight equation is corrected using structural optimization results. Even though the Grumman weight equation is more detailed in the parameters of geometry, the

variables are used for the rib cap areas, because they always tended to the minimum gage. Figure 3.2 shows the refined design variable set for the same design. We assume a uniform thickness or area distribution within each group in the two sets of design variables.

We applied Von Mises stress constraints to all the wing skin panel, spar and rib elements. The local buckling constraints are applied by assuming the skin panel dimension is specified and made of sandwich construction with a 0.75 inch honeycomb core (see Fig. 3.3). However the weight of the core material is neglected in the weight calculation.

The local buckling constraints for a single panel are expressed by the interaction equation (Ref. 51)

$$\lambda_{NCR} + {\lambda_{SH}}^2 \leq 1, \tag{3.5}$$

where λ_{NCR} is the buckling criterion under uniform normal forces in both x and y directions and λ_{SH} is the buckling criterion under shear force. They are given as

$$\lambda_{NCR} = \frac{\left(\frac{m^2}{a^2}\sigma_x + \frac{n^2}{b^2}\sigma_y\right)}{0.823D\left(\frac{m^2}{a^2} + \frac{n^2}{b^2}\right)^2}, \tag{3.6}$$

$$\lambda_{SH} = \frac{\sigma_{xy}b^2}{KD}, \tag{3.7}$$

$$D = \frac{E\left(4{t_s}^2 + 6t_s t_c + 3{t_c}^2\right)}{(1-\nu^2)} \quad , \tag{3.8}$$

where

a, b - panel dimensions in x and y directions,

m, n - numbers of half-waves in x and y directions,

σ_x, σ_y - normal stress in x and y directions,

σ_{xy} - shear stress,

K - a factor depending on a/b, for square panel, $K = 7.75$,

E - Young's modulus,

t_s - thickness of the skin face (assumed to be the same on both faces),

t_c - thickness of the honeycomb core.

Because the element size is usually larger than the panel size, the average stresses at the centers of the two triangular elements which comprise a rectangular panel are selected as σ_x, σ_y and σ_{xy} . A range of (1, 10) for m and n is used to find the maximum buckling criterion under combined forces.

The minimum gage of the wing skin thickness is 0.004 ft, and the minimum spar and rib cap areas is 0.005 ft^2. The properties of titanium used are given in Table 3.1.

Table 3.1. Titanium Properties and Allowable

E	16.0 10^6 psi
G	6.0 10^6 psi
ν	0.332
ρ	0.163 lb/in^3
$\sigma_{x_{yield}} = \sigma_{y_{yield}}$	91.8 10^3 psi
$\sigma_{xy_{yield}}$	53.0 10^3 psi
$\sigma_{x_{fatigue}} = \sigma_{y_{fatigue}}$	25.0 10^3 psi
$\sigma_{xy_{fatigue}}$	14.4 10^3 psi

3.2 Sequential Approximate Optimization

We use sequential linear programming to reduce computational cost incurred by repeating the finite element analysis procedure. This approach replaces the

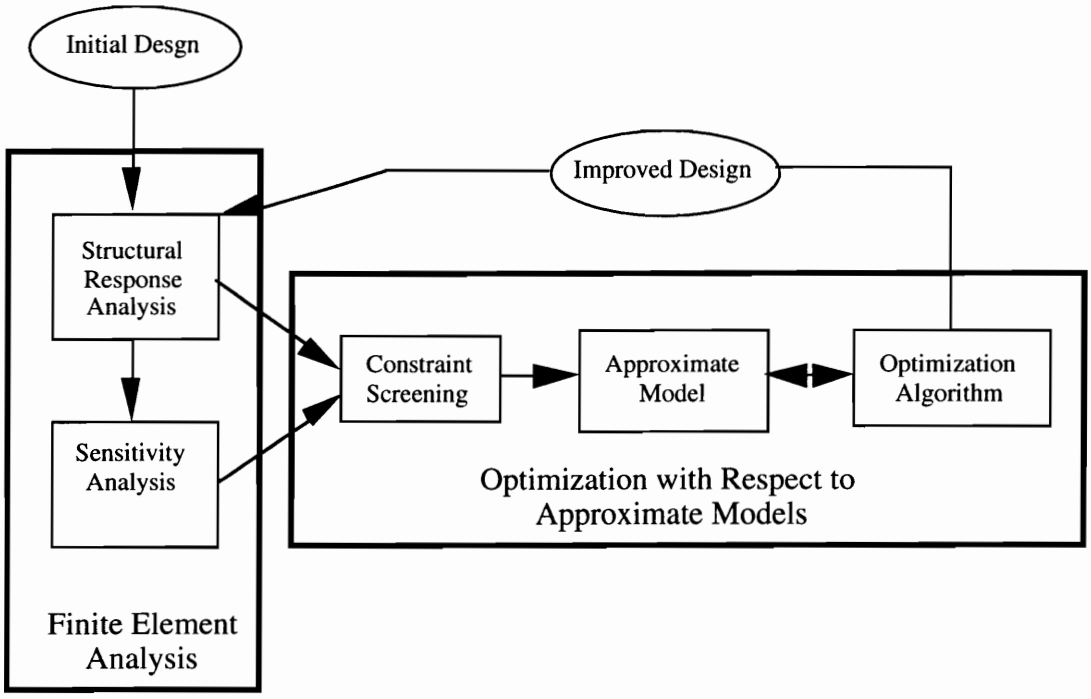

Figure 3.4 Sequential Approximate Optimization.

nonlinear objective and constraints with linear approximations based upon finite element responses and their sensitivities calculated at an initial design. The linear approximations to the objective function and constraints are much easier to evaluate and are much less expensive than the cost of a full finite element analysis. Therefore, the optimizer can request the evaluation of objective and constraint functions many times to solve this approximate problem. The approximation is valid when we stay close to the reference design for which the finite element analysis and the sensitivity analysis were determined. Move limits are used to prevent the design from moving outside the region of validity of the approximations. This approximate optimization is solved to produce an approximate optimum, and the procedure is called an optimization cycle. After an approximate optimum is found, a new approximation based on the new design is constructed and the procedure is repeated

until a convergent design is achieved. A typical starting move limit of 20 % is used, and it is decreased a little bit each optimization cycle. This procedure is illustrated in Fig. 3.4.

In our structural optimization, the stresses are calculated from the finite element analysis, and their sensitivities are calculated using finite differences with a fixed step size of 0.01%. The derivatives of aerodynamic and inertia loads are included using the procedure developed in Chapter 2. The Von Mises stresses, buckling criterion and their derivatives are then calculated as secondary responses. All constraints are normalized to a range of -1 to 1. Constraints with value of 1

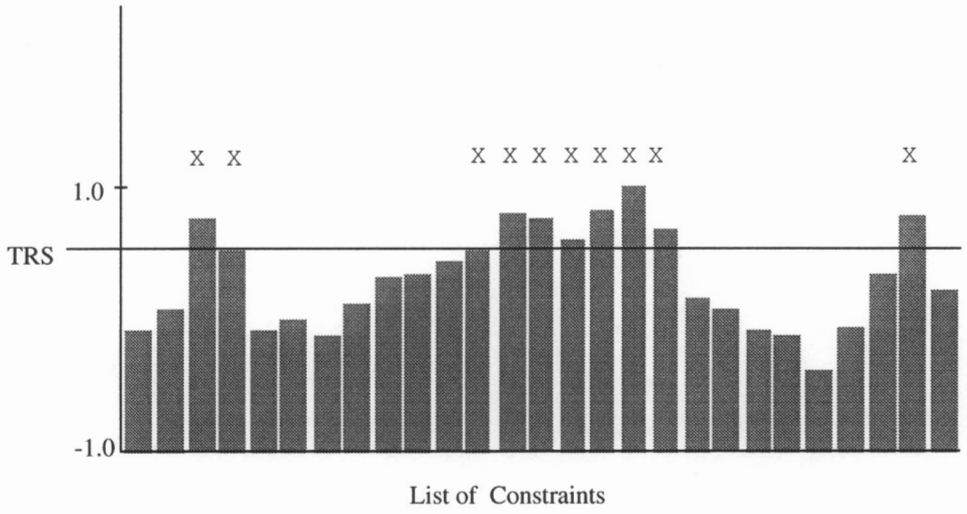

Figure 3.5 Constraint Screening.

or close to 1 can be considered as active. As the constraints are evaluated, they are dynamically screened by choosing a threshold value, TRS in Fig. 3.5, so that the number of constraints above or equal to this threshold level equals the number defined by the user. Only the constraints which are above or equal to the threshold level are flagged to be used in the optimization procedure. All of the other constraints are then discarded from consideration within this particular optimization cycle. Note that this screening procedure can be applied individually to each load

case or all the load cases; it can also be applied to each type of constraint or all types of constraints. The number of retained constraints should be at least twice the number of independent design variables. This screening procedure can reduce the computational cost for the optimization problem involving element level response such as stresses and/or strains.

3.3 Modeling and Loads

For consistency with the aerodynamic optimization procedure, a geometry format developed by Craidon (Ref. 40) in the early 1970's at NASA Langley Research Center is used to represent the aerodynamic design. The Craidon geometry defines the fuselage at a number of stations along the x-axis (see Fig. 3.6) by a collection of (y, z) data points. Similarly, the wing geometry is defined by airfoil cross sections at a number of spanwise locations. The engine nacelles (or pods) in the Craidon geometry are represented as axisymmetric bodies. Tail surfaces, fins and canards are assumed to be trapezoidal, with symmetric airfoil sections specified at the root and the tip of the surface. The coordinate axes used in Craidon geometry are illustrated in Fig. 3.3 and they are also the coordinate axes used in the finite element model.

The use of Craidon geometry enables the structural optimization to treat the aerodynamic optimization as a black box. Meanwhile, all the aerodynamic and structural analysis methods used in our work are programmed as individual routines or modules that depend only on the Craidon geometry to determine the characteristics of the configuration. Consequently, the analysis of a given design is independent of the design variables, once the geometry has been defined. This strategy minimizes the effort required to change the number or meaning of a set of design variables, and effectively isolates the analysis modules from the optimization

process. Thus, the individual techniques used to define an aircraft and estimate its performance are easily changed or upgraded without repeated overhauls of the entire analysis and optimization framework. The aerodynamic analysis programs or modules, such as the vortex-lattice and supersonic panel codes, can be used in the structural optimization directly without any change.

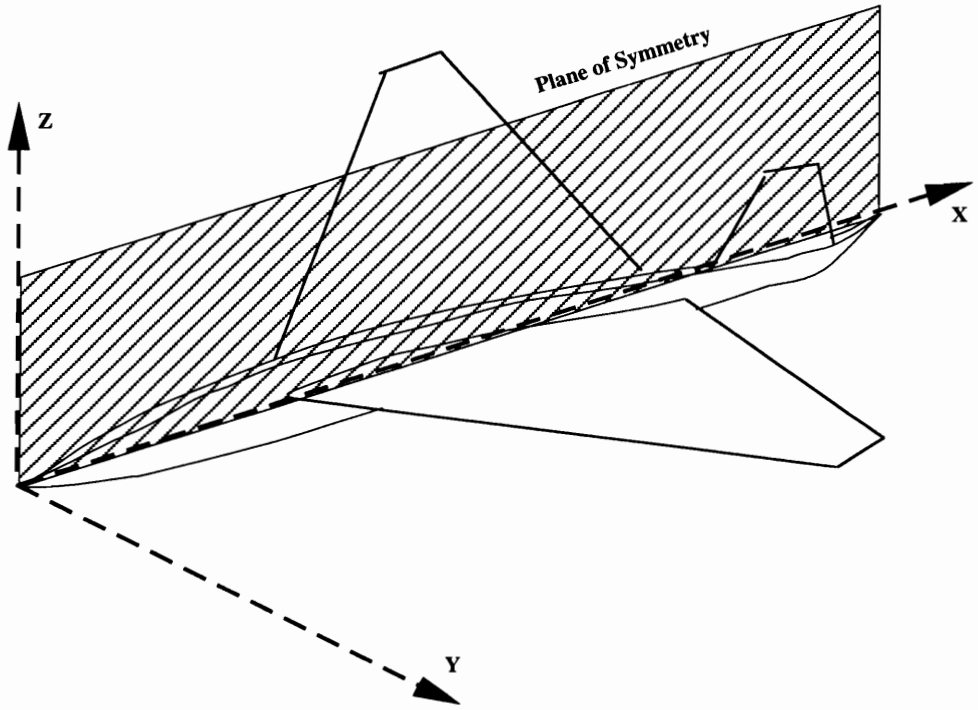

Figure 3.6 Coordinate System.

Rather than manually construct a finite element model for a given aerodynamic design, we developed a mesh generator to automate the procedure. Once the Craidon geometry is given, we need to specify the number of frames in the fuselage, the number of spars and ribs in the wing and the chord fractions taken by the leading and trailing-edge control surfaces. Instead of dealing with the three dimensional problem, the automatic mesh generator treats the whole aircraft as a two dimensional middle plane. At first this plane is divided into several regions such as fuselage, inboard wing, outboard wing and control surfaces. Then these regions are further divided into finite elements according to the given number of frames,

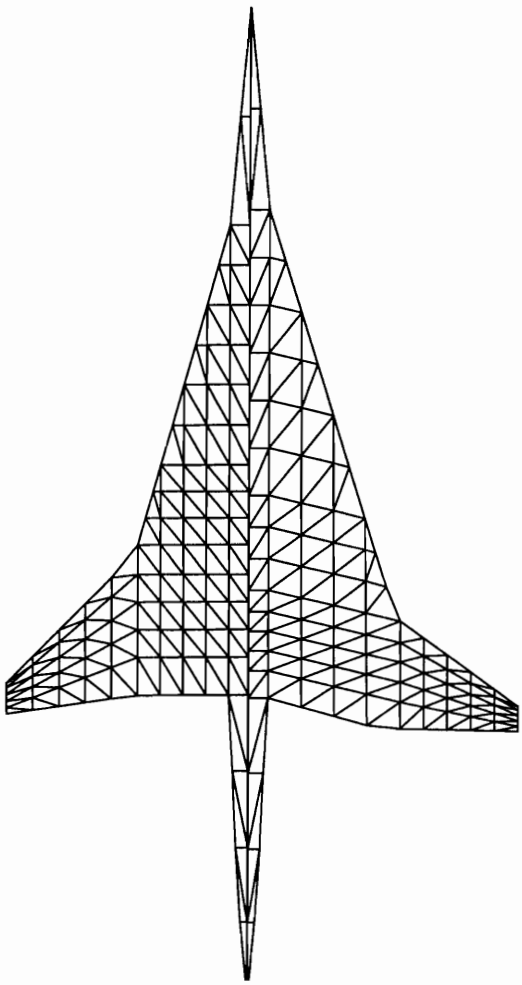

Figure 3.7 Finite Element Meshes from Automatic Model Generation for Two Different Planforms.

ribs, spars and the configuration requirement. Finally, a surface interpolation subroutine is used to split the middle plane mesh into the meshes of top and bottom surfaces. Figure 3.7 shows two typical finite element meshes automatically gener-

ated by this program. The left one is the finite element mesh used for the M2.4 baseline design and the right one is the finite element mesh used for a intermediate aerodynamic design. Besides the finite-element node coordinates and element topology data, the program also estimates the locations of all non-structural weights according to the planform geometry and a profile set up according to M2.4 baseline configuration. The volumes and locations of the wing fuel tanks are allocated by using the available space inside the wing and the rear part of the fuselage. The spar configuration generated by the program may be swept or cranked.

For consistency, the same numbers of fuselage frames, wing spar caps and wing rib caps are used in all the finite element models described in this work. The wing spars may be straight and swept or cranked so as to be orthogonal to the fuselage axis. According to Ref. 19, the swept spar model gives a slightly lighter structural design than the cranked spar model. However, we use cranked spar models for all the designs in our studies to allow more flexibitity in the planform geometry. The typical finite element models shown in Fig. 3.7 are made up of 923 elements joined at 193 nodes with 579 total degrees of freedom. A list of structural elements with corresponding number of finite elements used for each is given in Table 3.2. To facilitate the distribution of aerodynamic pressure and inertia loads to finite element nodes, both leading and trailing edge control surfaces are included in our model. The fuselage skin and frames were also modeled using large membrane and bar elements. The thicknesses and areas of those elements were chosen to match the estimated structural weight. Because of symmetry, we need to consider only a half-model of the aircraft. The boundary conditions specify symmetry of the displacements about the centerline. Supports were introduced to eliminate singularities in the stiffness

Table 3.2. Finite Element Model Break Down

Member	Number of Elements
Membrane	306
Shear Webs	168
Spar Caps	196
Rib Caps	178
Edge Rod	34
Vertical Rod	79

matrix. However, with the loads balanced to zero, all the reactions at these supports should be equal to zero.

Following Ref. 19, we considered 5 different load cases in the optimization, as shown in Table 3.3. The first two load cases were considered as fatigue load cases, and the last three load cases were considered as critical load cases. The factors of safety employed for each of these load cases are shown in Table 3.4.

Table 3.3. Structural Load Cases

Load Case	Load Factor	Mach Number	Dynamic Pressure (lb/ft^2)	Fuel Weight %
1. Mid-cruise	1.0	2.4	535	50
2. Transonic climb	1.0	1.2	644	90
3. Low-speed pull-up	2.5	0.6	367	95
4. High-speed pull-up	2.5	2.4	723	80
5. Taxi	1.5	0.0	0	100

Table 3.4. Constraint Safety Factors

	Load Cases 1 and 2	Load Cases 3, 4 and 5
Stress, strain	1.0	1.5
Buckling	1.5	2.25

3.4 Implementation

Figure 3.8 presents a graphical description of the general procedure of structural optimization developed in this study. The system was developed in the UNIX system using FORTRAN, C and EAL programming. The whole system is automatically connected together using C SHELL programming, and the user needs to provide the structural configuration data file and the flight condition data file. Because of modal approximation, the sizes of user input and intermediate files are much smaller than the EAL database.

As an engineering analysis language, the EAL program provides user extensive facilities for engineering computation, data management, graphic and tabular data display. The different processors in EAL are independent and they communicate with each other through a random-access database consisting of one or more libraries of named datasets. As each processor executes in response to the user's commands, it automatically extracts any required source datasets from the database and creates new datasets or modifies existing datasets. Processors do not have to be executed in any fixed order, provided that earlier processor executions have created all necessary source datasets. Restarting is totally automatic. The user simply re-attaches the file or files containing the database and resumes execution as though the prior run had not terminated. The flexibility allows us to run EAL, FORTRAN and C programs in the same database environment and use the datasets in the existing database, and this can save us a lot of computational time. For example, instead of performing a new normal mode analysis, we can update the initial design to the current design by updating the generalized mass and stiffness matrices using the database created by the previous normal mode analysis.

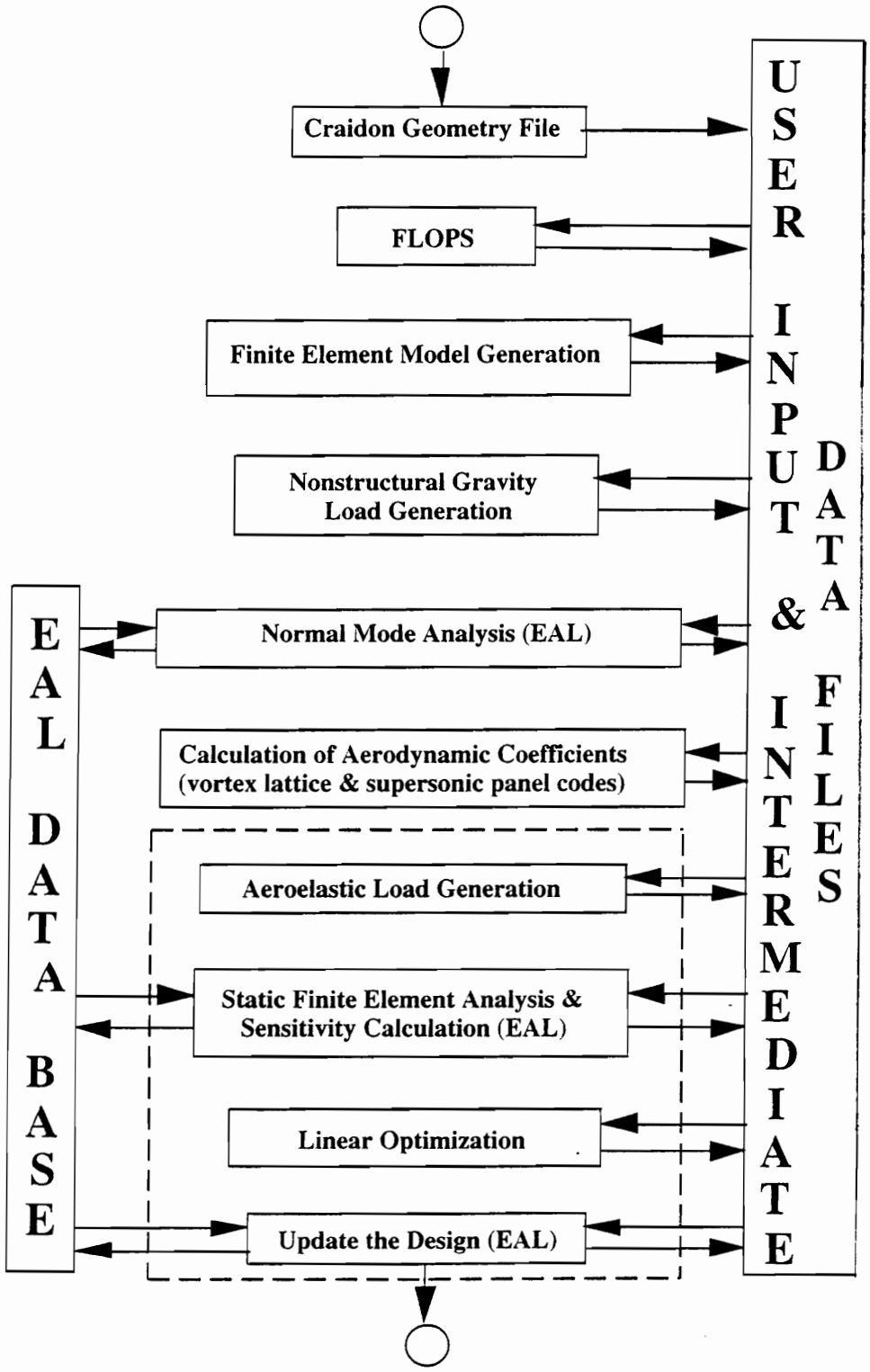

Figure 3.8 Flow Chart of Structural Optimization.

As mentioned before, the aerodynamics design was provided as a Craidon geometric file to the system. Then, FLOPS weight equations are used to estimate the structural and non-structural weights, except for the weight of wing bending material which is applied to the finite element model directly. We assume that the fuel is stored in 31 tanks: 3 in the aft section of the fuselage and 14 tanks in each wing. For the calculation of the nonstructural gravity loads, an initial fuel distribution is given, assuming that the ratios of fuel in each fuel tank over the maximum fuel capacity of the tank are the same. The normal mode analysis of the free aircraft is performed to provide the vibration frequencies and modes, mass, stiffness matrices and derivatives of mass and stiffness matrices with respect to the structural design variables. The unit mass matrix of each fuel tank is also calculated for fuel management. Vortex lattice and supersonic panel codes are then called to calculate the derivatives of aerodynamic loads with respect to angle of attack and vibration modes. The aerodynamic coefficient calculation and normal mode analysis procedures need to be performed only once, and this saves us considerable computational resources. The analysis procedures in the dashed frame are iterated in the sequential linear programming until a converged design is obtained.

The rigid loads are treated as a special case with the wing deformation set to zero.

3.5 Comparison with Equivalent Plate Model

As a first step, we performed a structural optimization on the M2.4 baseline design using the initial set of structural design variables and two rigid load cases (transonic climb and low-speed pull-up). Three sizes of skin panel were considered in our buckling constraint calculation. We compare our results with the results of Ref. 19 in Table 3.5. Unlike the wing bending material weight, the structural weights

Table 3.5. Comparison of Total Wing Skin Weights with Ref. 19.

Buckling Length (ft)	3.0	2.5	2.0	*
Ref. 19 Weight (lb)	69,862	57,894	50,260	
Ref. 19 Allowable and Loads	64,666	55,392	48,862	46,870
Ref. 19 Loads	59,776	51,004	43,712	43,704
Our Results	57,832	48,160	41,096	39,984

* No buckling constraints

shown in the table include the wing skin, the spar and rib caps of the wing box and the control surfaces. The weights in the last line are our optimization results and the weights in the first line are repeated from Ref. 19. As can be seen, our results are substantially lower than the corresponding results given in Ref. 19. To check on the possibility that our aerodynamic and inertia loads and stress and strain allowable were the source of the difference, we re-ran the optimization with the loads and allowables used in Ref. 19. The weights in the second line are our results using the loads and allowables of Ref. 19. The third line in the table shows the weights determined using the loads of Ref. 19, but our values for the allowable stresses and strains. Finally, the last line in the table shows the results obtained using only our analysis. Significant differences between the first and second lines reflect modeling differences (plate model versus finite-element model) and design variable differences. However, the majority of the difference is due to the choice of stress and stran allowables. Specifically, the analysis of Ref. 19 used $\sigma_{xy_{yield}} = 0.37\sigma_{x_{yield}}$, while we used $\sigma_{xy_{yield}} = 0.57\sigma_{x_{yield}}$. We feel that the values used in Ref. 19 were too conservative.

To check the effect of the number of design variables, we also defined a refined set of structural design variables described earlier and reoptimized the M2.4 baseline design using the refined design veriables. Table 3.6 compares the results obtained by using the initial and refined set of design variables. The comparison shows that the weight was reduced by as much as 24% solely by the introduction of the refined design variables set.

Table 3.6. Comparison of Total Wing Skin Weights Using Initial and Refined Design Variables.

Buckling Length (ft)	3.0	2.5	2.0	*
Initial Design Variables	57,832	48,160	41,096	39,984
Refined Design Variables	43,848	38,410	36,080	36,056

* No buckling constraints

3.6 Comparison of Rigid and Flexible Loads

Based on our preliminary results described in the last section, we keep the refined design variables in all the following work showed in this chapter and the next chapter, and we only discuss optimization results based on the five load cases in Table 3.2 with buckling length of 2.5' $\times$ 2.5'.

The importance of the static aeroelastic effects is evaluated by comparing the results of structural optimizations for rigid and for flexible loads. Several designs obtained during the course of aerodynamic optimization were optimized.

The first design we studied is the M2.4 baseline design. Figure 3.9 shows the convergence histories of the wing bending material weight for both rigid and flexible loads. Both convergence histories are very smooth and lead to almost identical final

designs. The final wing bending material weight with the rigid loads is 32,371 lbs., and the final wing bending material weight with the flexible loads is 31,485 lbs.. The difference is about 2.7%. The static aeroelastic effect on the structural weight is found to be very small and can be ignored without introducing large errors in this case.

To compare the difference between the final wing designs with rigid and flexible loads, the skin thickness distributions for both final designs are shown in Fig. 3.10. The same variable levels are used for the thickness distribution of both top and bottom covers of both final designs with rigid and flexible loads. The minimum value is 0.048 in and the maximum value is 0.35 in. We find that the primary wing box is the most critical part for the wing bending structural design, especially the region near the break between the inboard and the outboard wing sections. Even though there is a slight redistribution of material, the thickness distributions for both the final wing design are very similar. The area distributions for spar caps are also very similar and the all rib cap areas go to minimum gage.

Figure 3.11 gives the active load cases for both final designs. The b's in Fig. 3.11 indicate that the buckling constraint is active in the marked region. The notation load case 0, none, means that there are no active constraints in the region. We find that only transonic climb, load case 2, and low-speed pull-up, load case 3, among the five load cases, control the design variables. Actually, both Von Mises stress constraints in transonic climb and low-speed pull-up load cases and buckling constraints in the low-speed pull-up load case are active in the region near the break between the inboard and the outboard wing sections. However, the transonic climb constraints are slightly more critical.

To check whether the static aeroelastic effects can be ignored in other cases, we also optimized several designs using both rigid and flexible loads. The largest

difference in final wing bending material weight of about 7.0% was obtained for a highly swept wing. Figure 3.12 shows the convergence histories of wing bending material weight which gave the largest difference. Figure 3.13 presents the thickness distributions for both the final designs with rigid and flexible loads. We can see that there are slight differences in the thickness distributions. As shown in Fig. 3.14, both the transonic climb and low-speed pull-up load cases are active on the top skin of this design. However, only the transonic climb load case is active on the bottom skin of this design, and this allows the optimizer to take more advantage of changing the load distribution.

For the wing design with rigid loads we typically found that only two load cases were critical. However, for the wing design with flexible loads, it is dangerous to work with a small number of load cases. With the loading depending on the design variables, the optimizer can reduce stress not only by adding material, but also by changing the load distribution. This strategy can be particularly effective when only one or two load cases are used. Figure 3.15 demonstrates the effect of the number of load cases for an arrow wing design. The figure compares the convergence histories of wing bending material weight using two load cases (transonic climb and low-speed pull-up) with that using all five load cases. It is seen that the wing design with flexible loads can achieve substantially lower weight with 2 load cases, even though they are the most critical load cases for the wing design with rigid loads. Because even 5 load cases is a small number, the results with flexible loads may be unconservative. Using structural optimization with rigid loads appears to be a conservative estimate of the effect of the geometric changes on the structural weight.

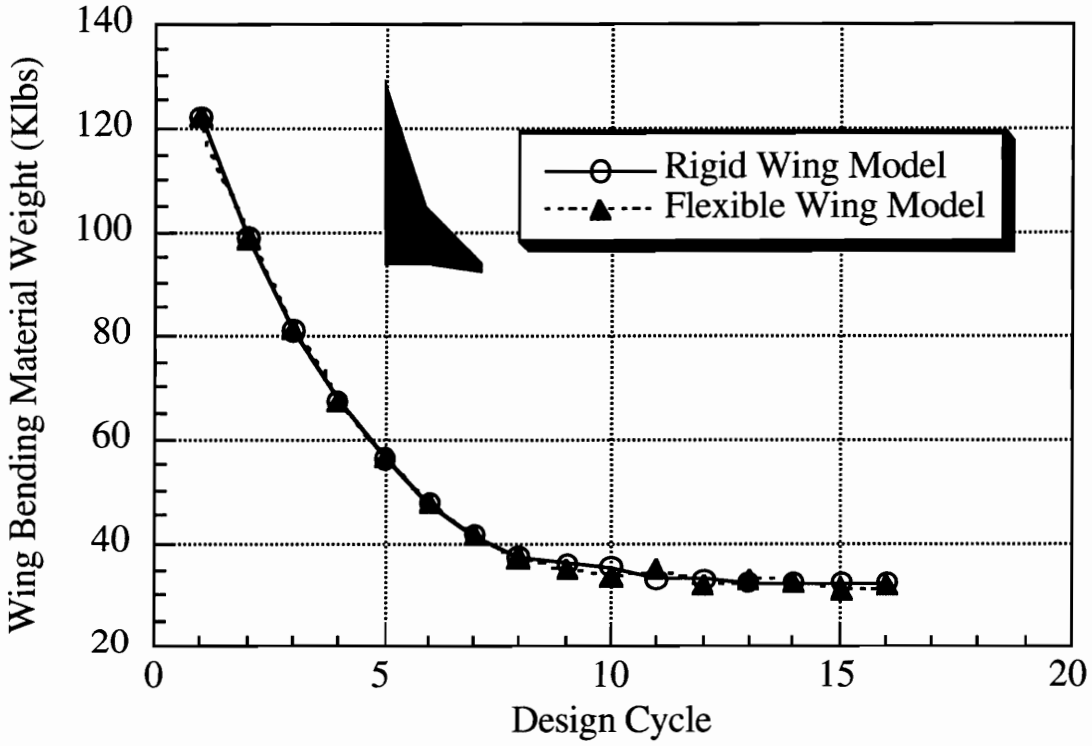

Figure 3.9 Wing Bending Material Weight Convergence for M2.4 Baseline Design.

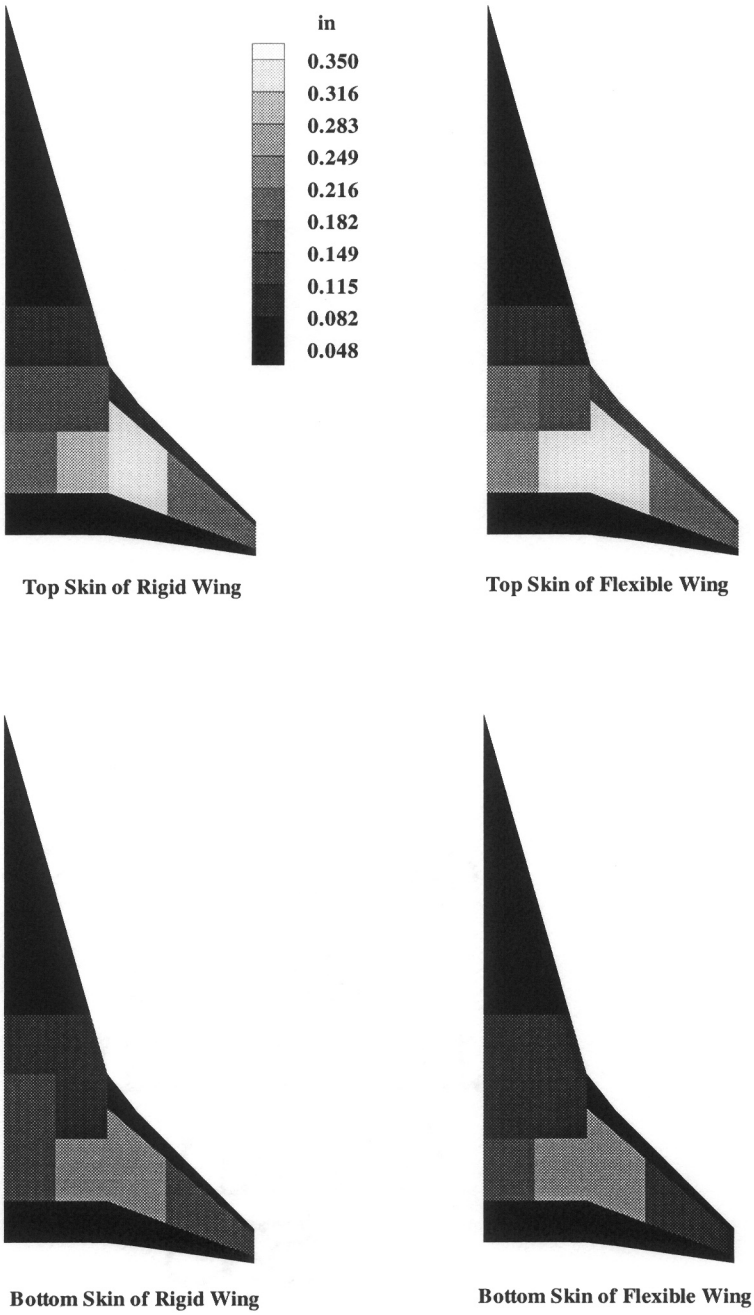

Figure 3.10 Skin Thickness Distribution for M2.4 Baseline Design

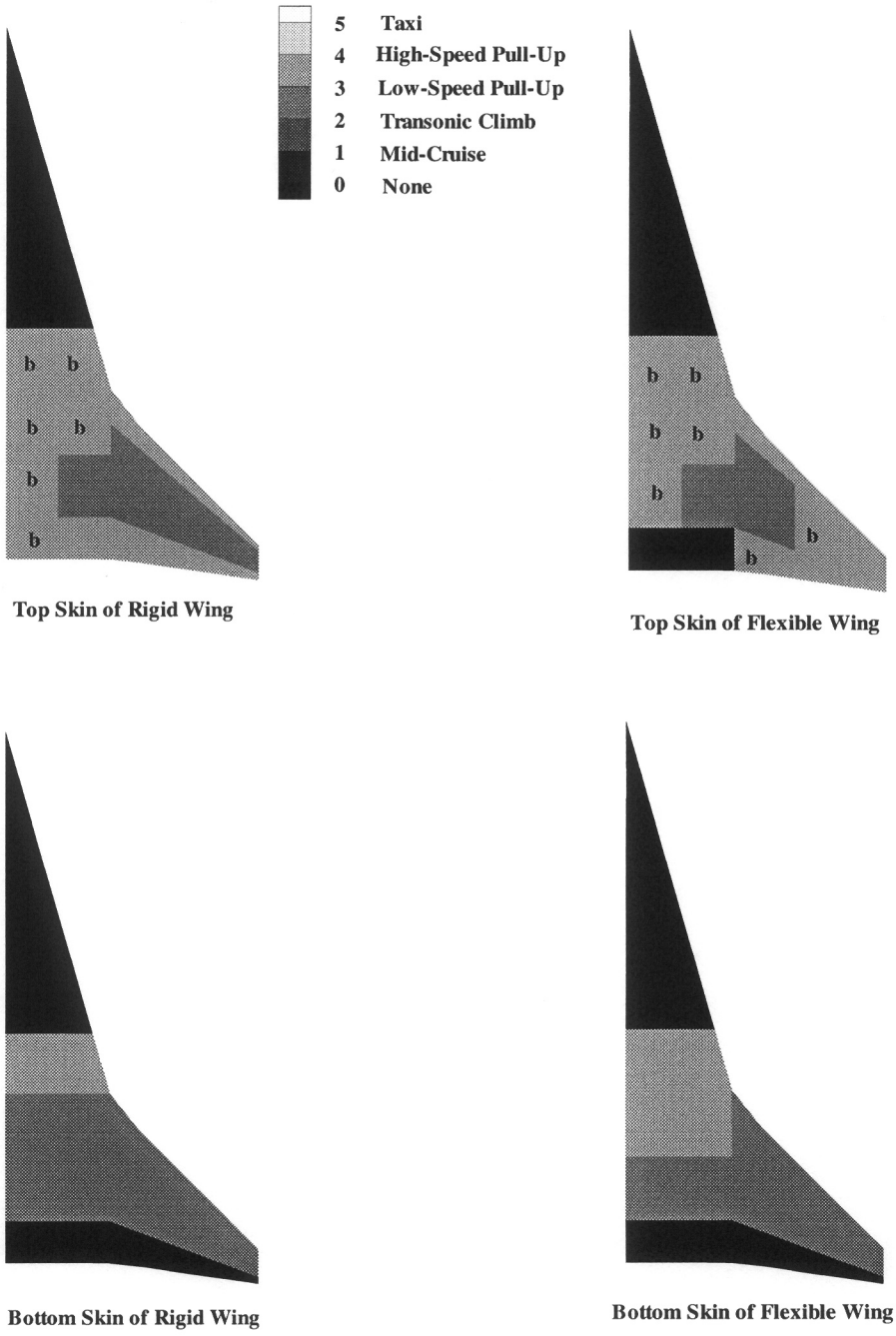

Figure 3.11 Active Load Cases for M2.4 Baseline Design

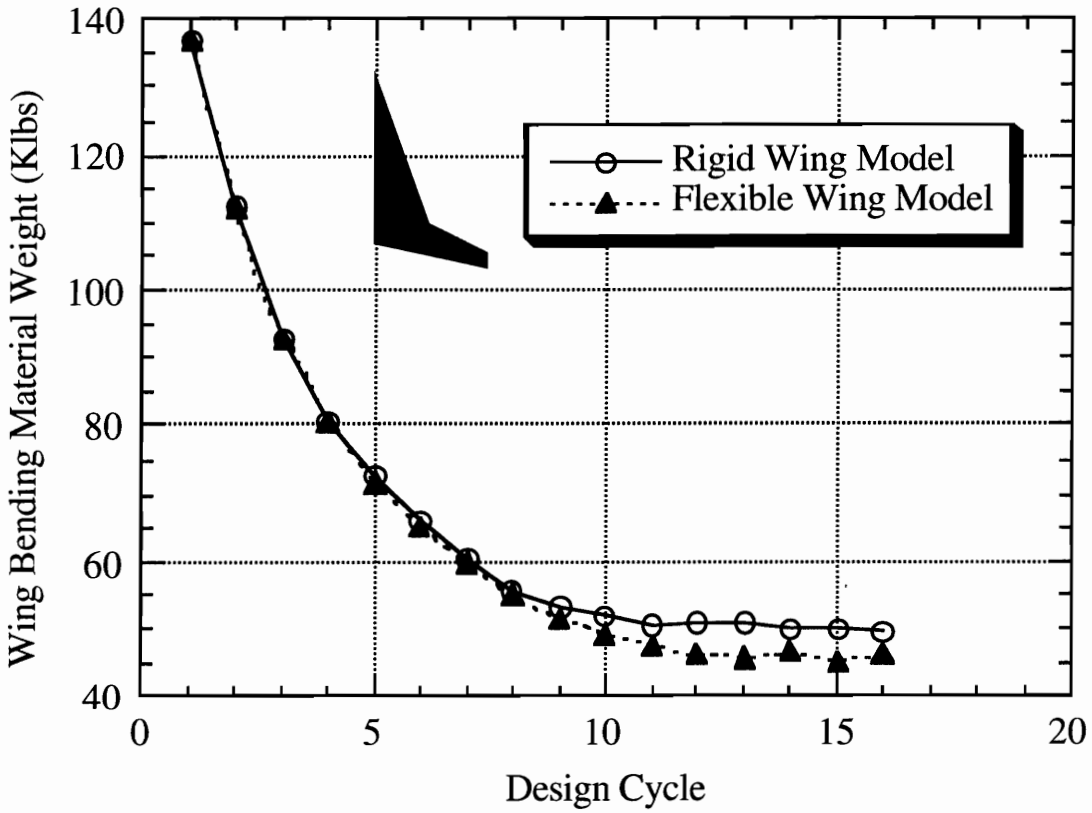

Figure 3.12 Wing Bending Material Weight Convergence for a Highly Swept Wing Design

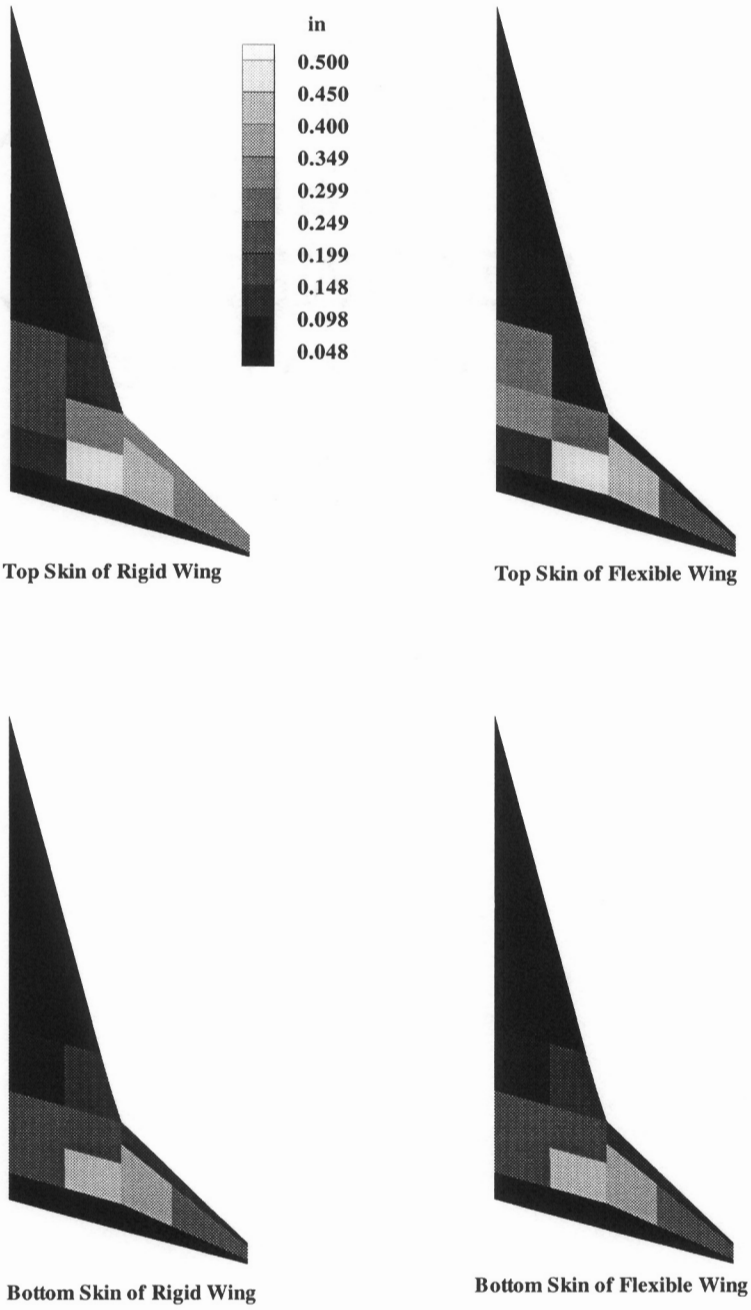

Figure 3.13 Skin Thickness Distribution for Highly Swept Wing Design

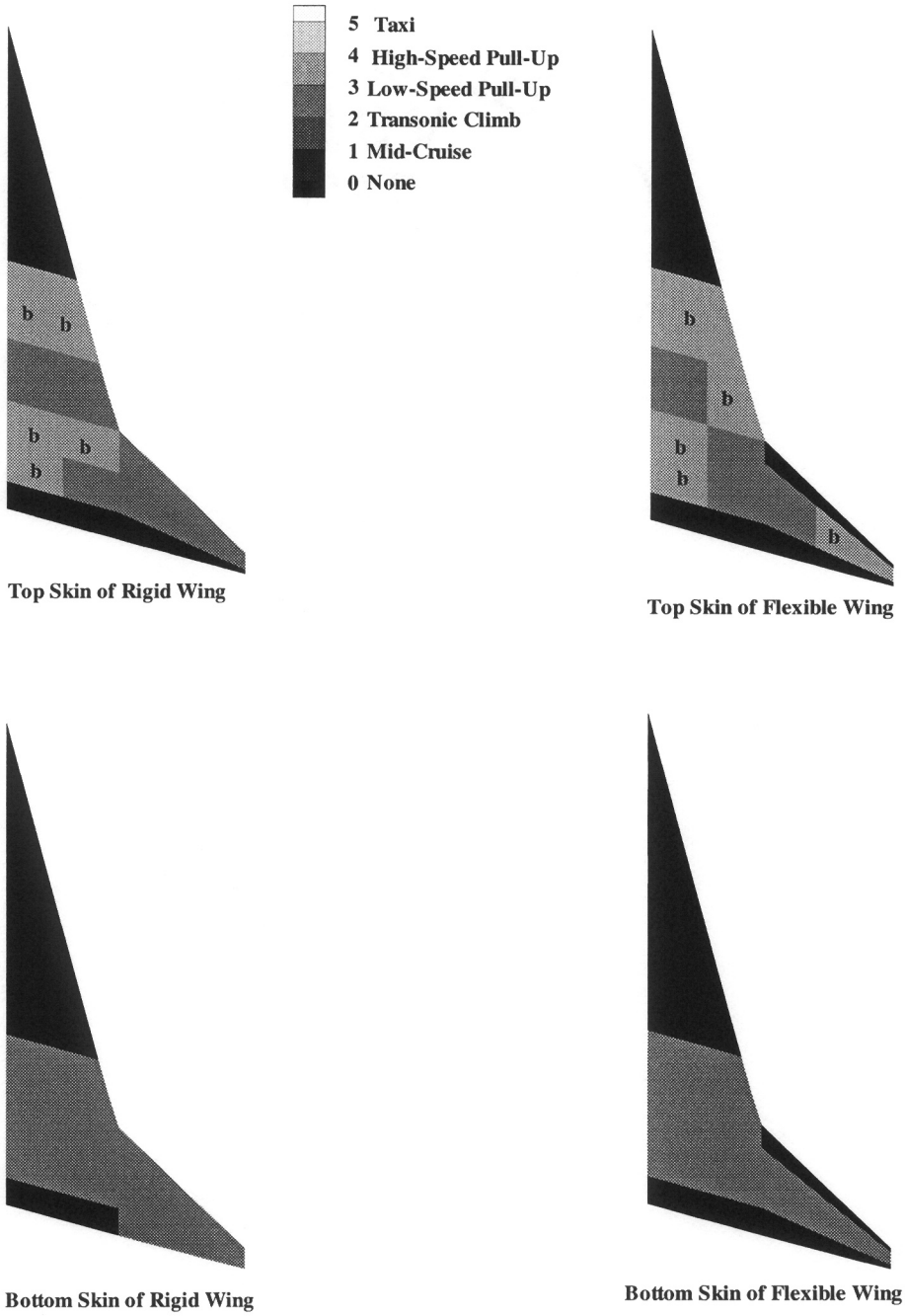

Figure 3.14 Active Load Cases for Highly Swept Wing Design

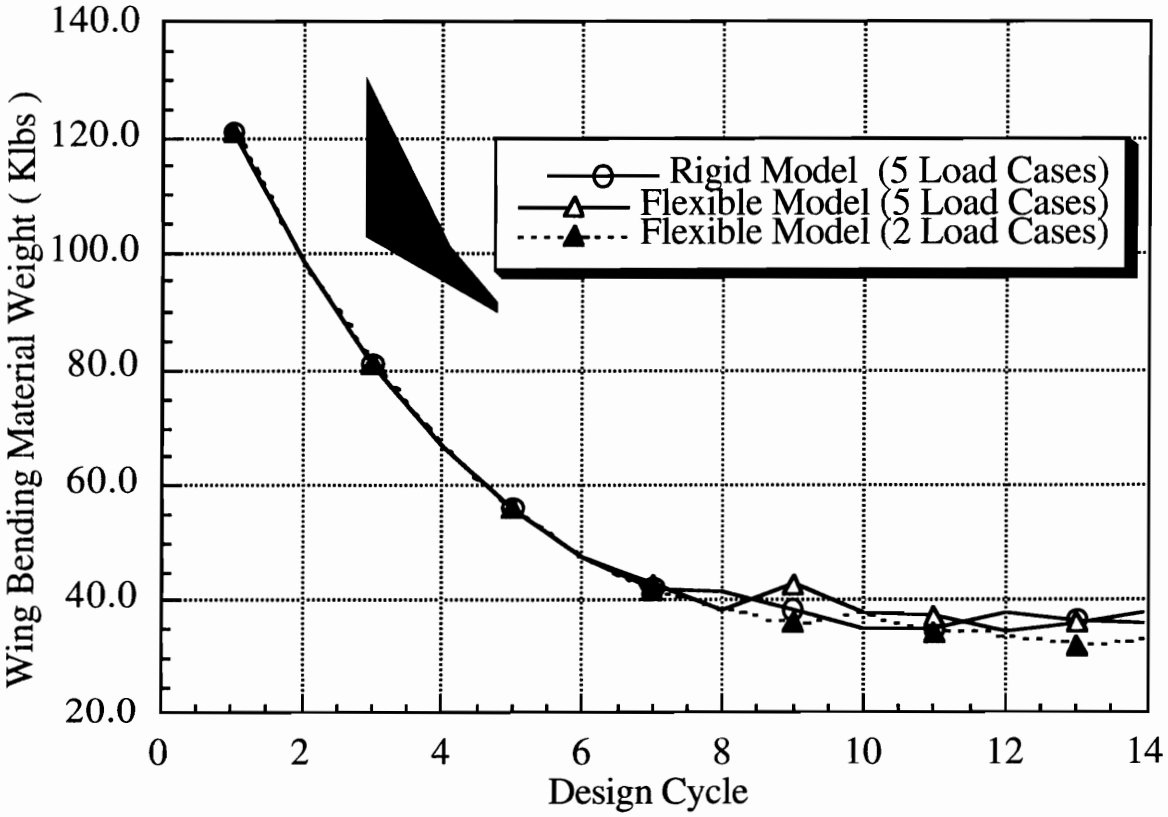

Figure 3.15 Wing Bending Material Weight Convergence Using Different Numbers of Load Cases.

4. Weight Equations and Interlacing Procedure

The finite-element-model based structural optimization described in the last chapter provides us with an accurate method for estimating the wing bending material weight and the effect of change in geometry on that weight. However, this approach is computationally expensive compared to simple statistical weight equations that are used in conceptual design programs such as FLOPS. This large computational cost may make the use of structural optimization impractical for combined multidisciplinary design. Moreover, the finite-element-based structural optimization procedure can provide us with estimates of only wing structural weight, and we still need weight equations to estimate other component weights. In this chapter, we evaluate the weight equations used in the aerodynamic optimization by comparing them with structural optimization results. We then explore an interlacing procedure to combine the efficiency of simple weight equations with the accuracy of finite-element-model based structural optimization. Results obtained with aerodynamic optimization using this procedure are presented to validate this approach.

4.1 Weight Equations

Simple statistical weight equations are commonly used in the preliminary stage of advanced aircraft design (e.g., Refs. 52, 53). They are developed based on a data base of existing aircrafts using statistical methods. Most of the aircraft in the data base are subsonic and have high aspect ratio wings. Therefore these weight equations may not account for all features of new advanced supersonic aircraft with low aspect ratio wings, such as the high speed civil transport.

Most of the load-dependent wing weight is due to bending, and so the bending material weights given by weight equations were compared to the weight predicted by structural optimization. Two wing bending material weight equations will be discussed in this section. The first weight equation developed by McCullers is taken from FLOPS (Ref. 12) which was used in our aerodynamic optimization. The second weight equation is given by a Grumman Aerospace Corp. contractor report (Ref. 54) and is used to avoid conclusions that reflect the idiosyncrasies of one weight equation.

FLOPS Weight Equation

The wing weight equation in FLOPS is based on an analytical expression to relate wing bending material weight to primary configuration parameters such as aspect ratio, thickness-chord ratio, etc. (Ref. 55). Terms were added to account for shear material, control surfaces, leading and trailing edges, etc. Then, constant factors were used to correlate with a wide range of existing transports and to include features such as composite materials, strut-braced wings, etc. The wing weight W_w is given as

$$W_w = \frac{W_g C W_b + W_s + W_n}{1 + W_b}, \tag{4.1}$$

where

$$W_b = C f_{ul} b (1 - 0.4 f_c)(1 - 0.1 f_a), \tag{4.2}$$

$$W_s = 0.68(1 - 0.17 f_c)(S - S_b)^{0.34} W_g^{0.6}, \tag{4.3}$$

$$W_n = 0.35(1 - 0.30 f_c) S^{1.5} \tag{4.4}$$

$$C = 8.8B_t[1 + (\frac{6.25}{b})^{\frac{1}{2}}] \times 10^{-6}, \tag{4.5}$$

and

W_w - total wing weight (lbs),

W_b - wing bending material weight (lbs),

W_s - wing shear material and flaps weight (lbs),

W_n - wing control surfaces and non-structural weight (lbs),

W_g - take-off gross weight (lbs),

b - wing span (ft),

S_b - wing box area (ft^2),

S - wing area (ft^2),

f_{ul} - ultimate load factor,

f_c - composite material factor,

f_a - aeroelastic tailoring factor,

B_t - bending material factor,

This equation is closed except for the bending material factor B_t. This term accounts for the distribution of the load on the wing. It is calculated by approximately determining the required material volume of the upper and lower skins in a simple wing box description of the wing. We begin by finding the weighted average sweep angle at 75% chord locations:

$$\Lambda_L = \int_0^1 (1 + 2y)\Lambda(y)dy. \tag{4.6}$$

An idealized simple elliptic distributed pressure load is assumed to determine the bending moment:

$$p(\xi) = (1 - \xi^2)^{1/2}, \tag{4.7}$$

$$M(y) = \int_0^y p(\xi)\xi d\xi. \tag{4.8}$$

With this bending moment distribution it is possible to calculate the necessary flange area as

$$A(y) = \frac{M(y)}{t(y)c(y)cos\Lambda(y)}, \tag{4.9}$$

and the required material volume as

$$V = \int_0^1 A(y)dy. \tag{4.10}$$

The total lift load is

$$L = \int_0^1 p(y)dy, \tag{4.11}$$

and the bending material factor is finally given as

$$B_t = \frac{2V}{Ld}, \tag{4.12}$$

where

$$d = AR^{0.25}[1 + (0.5f_a - 0.16)sin^2\Lambda_L + 0.3C_y(1 - 0.5f_a)sin\Lambda_L], \tag{4.13}$$

and

$$C_y = 0 \text{ if } AR \leq 5 \text{ and } C_y = AR - 5 \text{ if } AR \geq 5.$$

Grumman Weight Equation

The Grumman weight equation is more detailed than the FLOPS weight equation in the geometric description. A theoretical wing weight equation was derived using a straightforward beam model with simple uniform loads. Then, this simple theoretical equation was modified using a least squares fit utilizing a data base of 50 actual airplane wing weights. Factors representing materials and method of construction were derived and incorporated into the basic wing bending material equation. Weight penalties due to fuel, engines, landing gear, stores and fold or pivot were also included. It finally gives the wing bending material weight as

$$W_b = 0.468492[\frac{b(C_r + 2C_t)W_e f_{ul} S}{cos^2\Theta(C_r + C_t)(2T_r + T_t)(2C_r + C_t)}] \times S_b^{0.5279} V_l^{0.1634} f_f f_m f_t, \tag{4.14}$$

where

C_r - wing root chord (ft),

C_t - wing tip chord (ft),

T_r - wing root airfoil maximum thickness (ft),

T_t - wing tip airfoil maximum thickness (ft),

W_e - total aircraft weight without fuel (lbs),

Θ - sweep angle at 40% chord (rad),

V_l - limit speed (knot EAS),

f_f - cover fail-safe factor,

f_m - cover material/construction factor,

f_t - cover temperature effect factor,

and the remaining terms are the same as these in the FLOPS weight equation.

4.2 Comparison with Structural Optimization

The weight predicted by the above wing bending material weight equations will be compared against the finite element model based structural optimization results. Because our work showed that the static aeroelastic effects are quite small for high-speed civil transport design, rigid loads are used for the structural optimization procedure. For our titanium high-speed civil transport design, we set f_c and f_a equal to 0 in FLOPS. The factors f_f, f_m and f_t are all set to 1.0 in the Grumman weight equation. The ultimate load factor, f_{ul} is set to 3.75 in both weight equations.

Figure 4.1 gives the planforms of ten aerodynamic designs used for this comparison study. The first design is the Mach 2.4 high-speed civil transport baseline design. The others are intermediate designs we obtained in the course of several aerodynamic optimization studies.

Figure 4.2 summarizes the structural optimization results and the estimations of FLOPS and Grumman weight equations for the ten designs. The average wing bending material weights predicted by the structural optimization, FLOPS and Grumman weight equations are 38017, 32454 and 45848 lbs., respectively. The FLOPS weight tends to underestimate the wing bending material weight while the Grumman weight equation tends to overestimate the wing bending material weight. The ratios of the weight predicted by structural optimization to the FLOPS weight equation varied between 0.93 and 1.50, while the ratios between the weight predicted by structural optimization and that of the Grumman weight equation varied between 0.59 and 1.18. Since optimization is concerned with the changes in weight due to changes in geometry, we also calculated the correlation coefficients between the two weight equations and the structural optimization procedure using

$$R_{xy} = \frac{\sum(x_i - \bar{x})(y_i - \bar{y})}{\sqrt{[\sum(x_i - \bar{x})^2][\sum(y_i - \bar{y})^2]}},$$

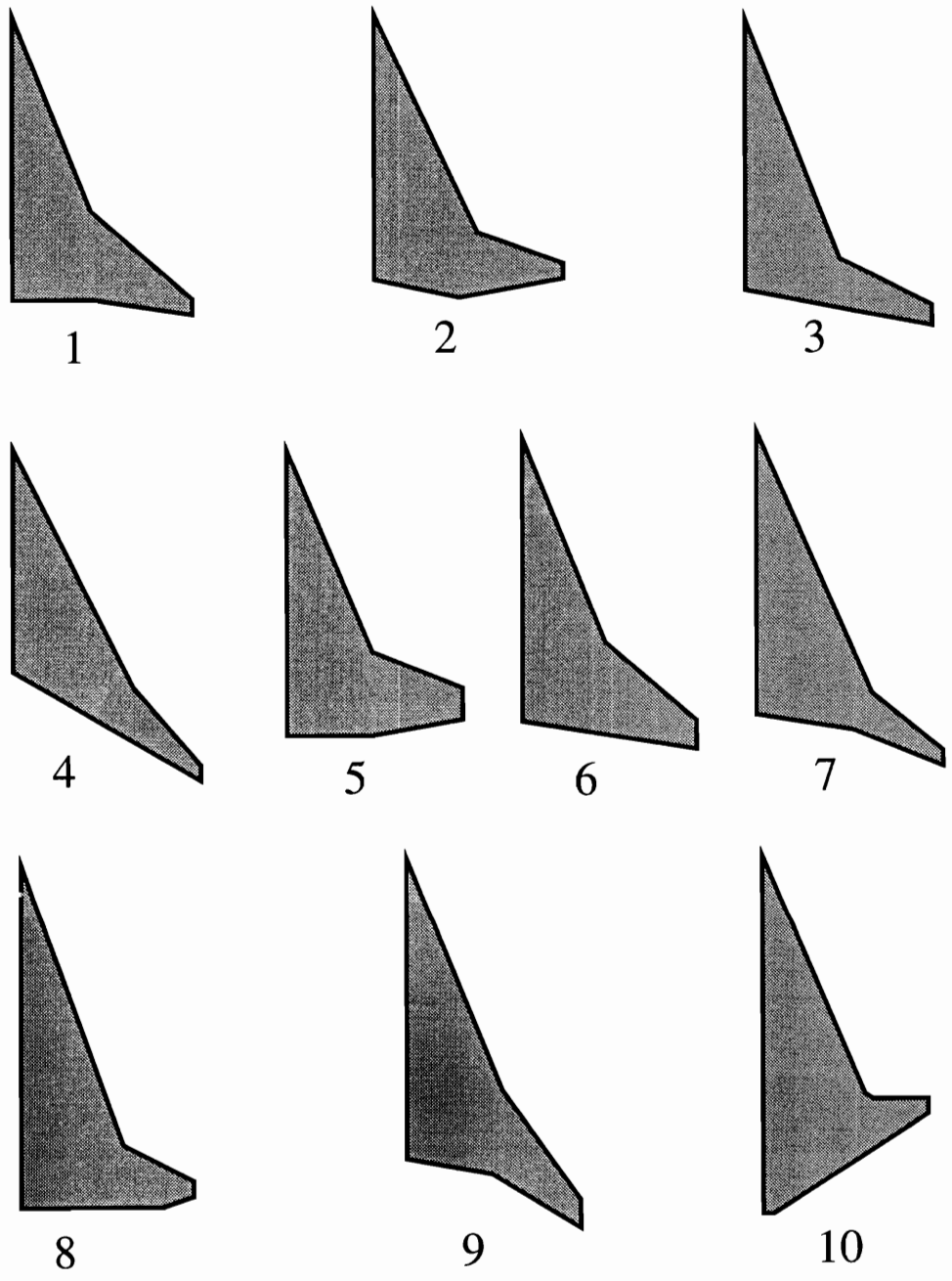

Figure 4.1 Planforms for Weight Equation Comparison Study.

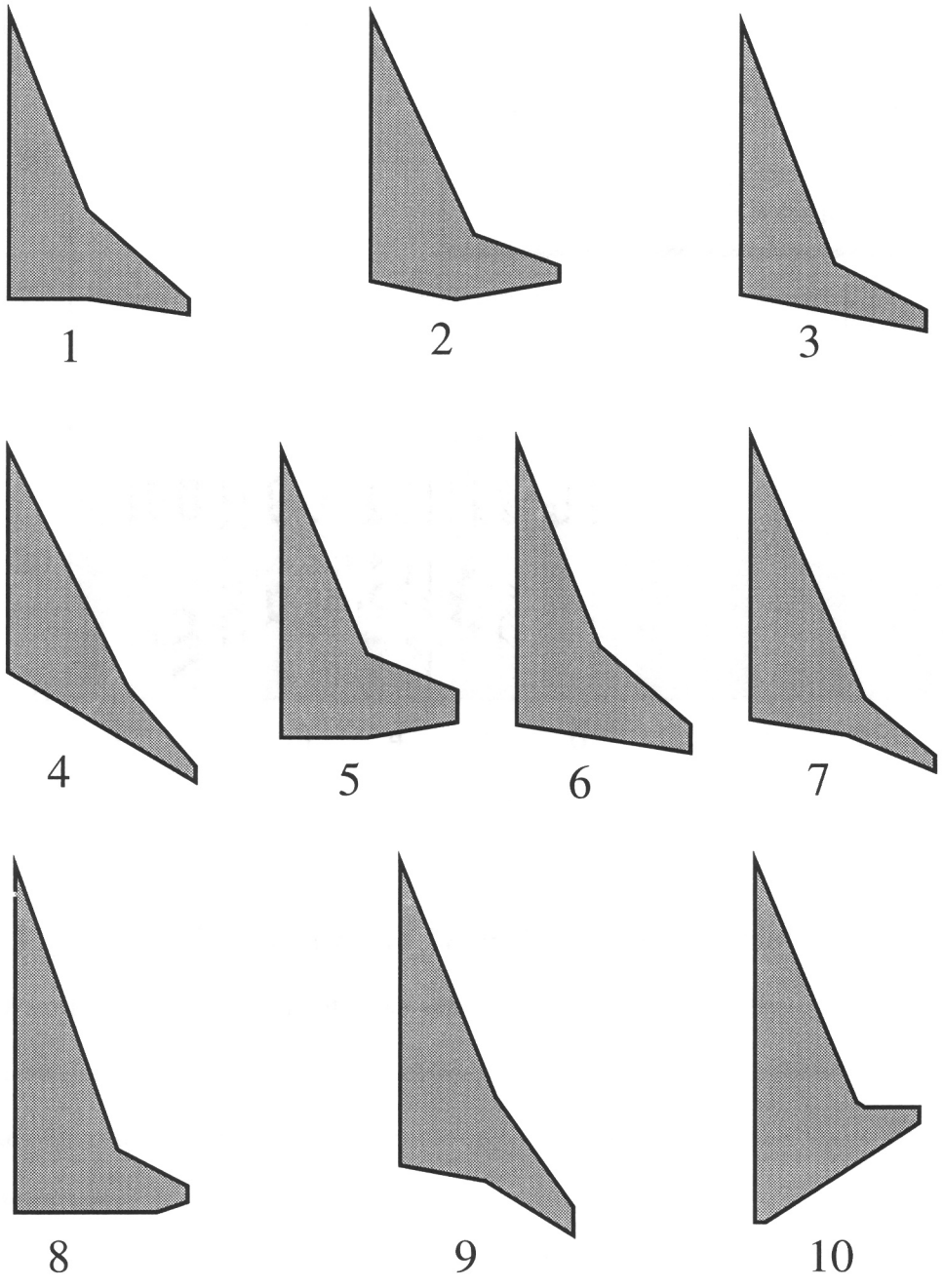

Figure 4.1 Planforms for Weight Equation Comparison Study.

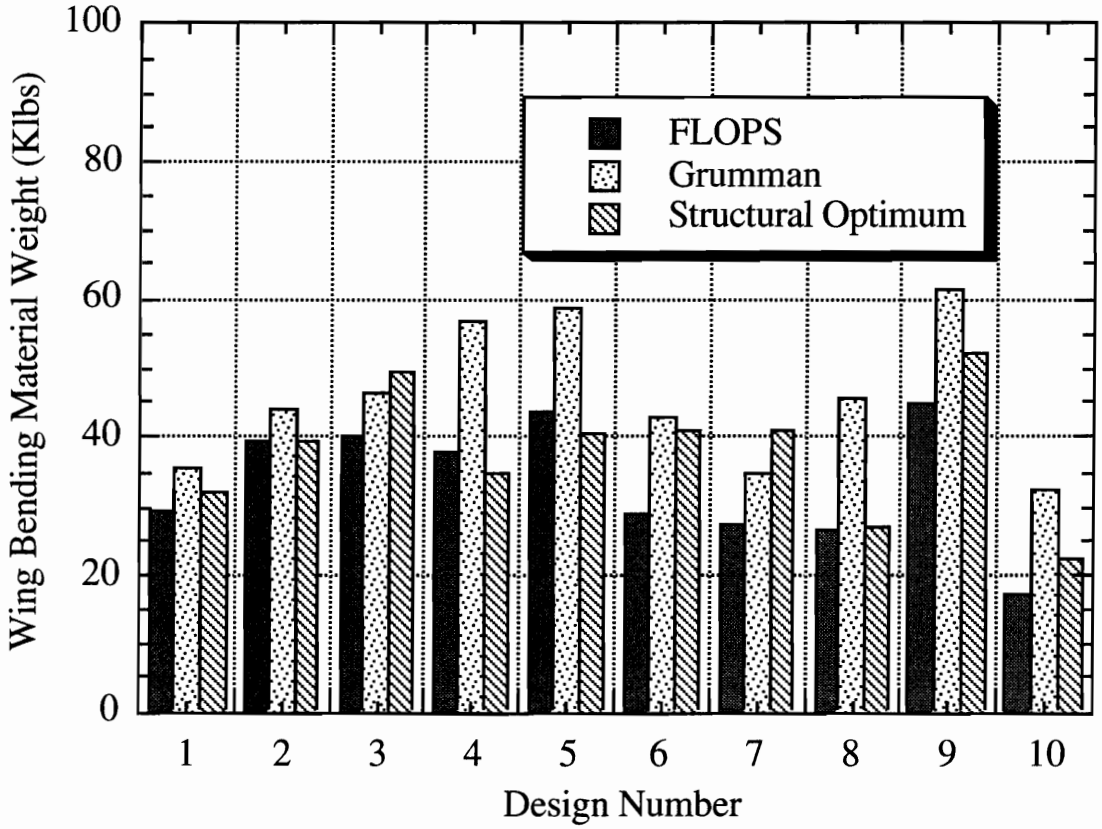

Figure 4.2 Comparison of Wing Bending Material Weight.

where $\bar{x}$ and $\bar{y}$ are the means of data sets x_i and y_i, respectively.

These correlation coefficients between two sets of data measure to what extent they increase or decrease in synchrony. We found that the three correlation coefficients were

$$R_{FG} = -0.05,$$

$$R_{FS} = 0.78,$$

$$R_{GS} = -0.34,$$

FLOPS weight equation achieves much better agreement with the structural optimization. This may be due to the fact that some structural optimization results for advanced aircraft designs were included in the data base of FLOPS, and the FLOPS weight equation was set up for transports while the Grumman weight equation was set up for military aircrafts. Based on this, we selected the FLOPS weight equation in the following interlacing procedure.

4.3 Interlacing Procedure

Aerodynamic design optimization with a structural weight equation captures the major effects of aerodynamic shape on structural weight. But weight equations cannot account for all features of a new design such as the high-speed civil transport. On the other hand, finite-element-model-based structural optimization procedures can overcome this deficiency, but are much more expensive in comparison with the statistical-data-based weight equation and can only provide the structural part of the aircraft gross weight. A full integration of the structural and aerodynamic optimization is computationally expensive due to repeated calculation of aerodynamic loads and derivatives of these loads with respect to all the aerodynamic design variables. As an intermediate step, we have implemented a variable-complexity-modeling strategy to interlace the aerodynamic and structural optimizations.

The relationship of aerodynamic and structural optimization in this procedure is given in Fig. 4.3. An aerodynamic design is chosen as a starting point. We apply the FLOPS weight equation to this aerodynamic design to get an estimate of the wing bending material weight W_{fb}.0 We obtain W_{ob} from structural optimization, and we define the interlacing factor as $s = W_{ob}/W_{fb}$. Next, we start the aerodynamic design optimization by using the FLOPS weight equation with the wing bending material weight multiplied by s. The aerodynamic optimization is

performed for several cycles with this interlacing factor fixed. Then, the interlacing factor, s, is updated by repeating the structural optimization. This procedure was repeated until the design converged. This procedure corrects the wing bending material weight provided to the aerodynamic optimizer, and prevents the aerodynamic optimization from obtaining unrealistic designs. However, because no information on the derivatives of the interlacing factor are provided, the optimizer may not be able to easily find good designs.

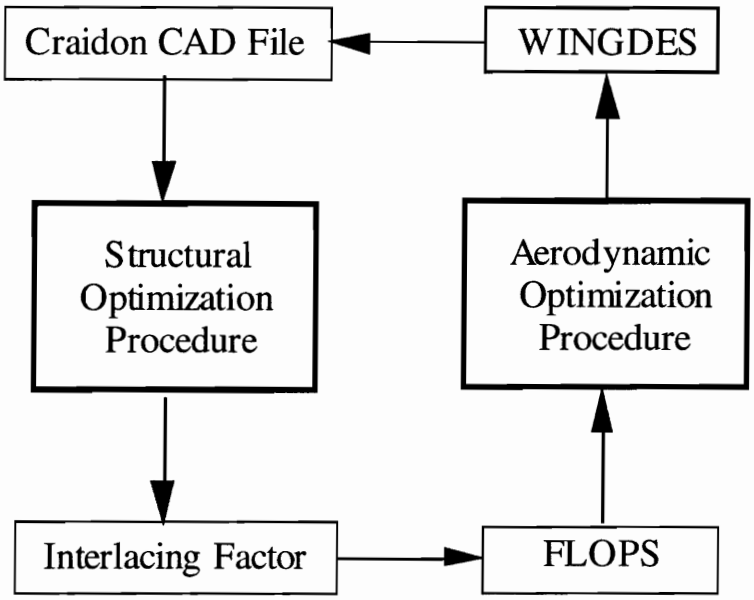

Figure 4.3 Interlacing of Structural and Aerodynamic Optimization.

4.4 Optimization Results with Interlacing

The interlacing procedure described above is applied to three different initial designs, each of which was first optimized without interlacing. The first two initial designs are intermediate aerodynamic designs obtained during the aerodynamic optimization procedure and the third one is an average design of first two. Figures 4.4 to 4.6 each show planforms of the initial design, the optimum design without interlacing and the optimum design with interlacing, for Case 1 to Case 3, respectively. Some important design characteristics are compared in Tables 4.2 to 4.4.

The ranges listed in the tables were the calculated ranges. For a better design comparison, the weights listed are the original weights corrected for any range deficiency, i.e., a range of less than 5500 n.mi., by the addition of 90 lbs. of fuel per mile range deficiency. The wing weight in the final designs with interlacing are already corrected by structural optimization results, and the wing weights of the initial and final designs without interlacing are original weights predicted by FLOPS weight equation.

These three cases represent a phenomenon repeatedly encountered in the aerodynamic optimization (Ref. 56). Noisy aerodynamic drag calculation (Ref. 57) created multiple local optima in design space so that final design strongly depended on initial designs. For case 1, both optimum designs produced without and with interlacing have an arrow-like wing. The final design with interlacing is a lighter aircraft with thinner airfoil and less drag, so it can be said to be a better aerodynamic design. In case 2, both with and without interlacing, the optimizer moved to an unusual planform. The planforms of the final designs appeared to be good structural designs. According to FLOPS weight equation, the wing bending material weight of final design without interlacing at 18199 lbs., is 31% lighter than the wing bending material weight of case 1 final design without interlacing. However, the structural optimization predicted only 1% saving. The FLOPS weight equation seems to be too optimistic in this case, and the aerodynamic optimizer took advantage of weaknesses in the FLOPS weight equation. The interlacing process tried to produce an even better structural design by increasing airfoil thickness and geometric size. However, the penalty associated with this strategy is larger than the benefit. The interlacing procedure produced a heavier design due to the increase of fuel weight. The planforms of the final designs we got in case 3 are similar to the final planforms obtained in case 1. However, instead of reducing the airfoil thickness to achieve the

efficiency of aerodynamic performance, the optimizer simply added fuel to satisfy the range constraint and ended up with a heavier design. Obviously, the noise of aerodynamic performance blocked the aerodynamic optimizer from better designs.

Figures 4.7 to 4.9 give the convergence histories of the total take-off gross weight. Large move limits are used in the aerodynamic optimization to escape the multiple local minima created by the noise. Because large move limits, e.g. 40% or more, are used in the first cycle, large variations appeared in all three convergence histories. The interlacing factor in the first case remained close to 1.0, moving only once as far as 1.2. The same situation existed in the case 3. When the interlacing factor is close to 1, the aerodynamic optimizer is effective, because the FLOPS weight equation is accurate. In the second case, the interlacing factor quickly approached 1.5 and remained near there, which mirrors the evolution of the planform. As in the non-interlaced optimization of this case, the optimizer, given initially large move limits, moved in one cycle to a planform similar to the ending planform shown, and did not move back into a region of the design space that "contained"the starting planform. (This is to be expected, since after one cycle the move limits were reduced from 40 % to 10 % and less). From Fig. 4.8 it can be seen that the space into which the optimizer moved the design was one in which the FLOPS weight was not very accurate. The failure of the optimizer to move out of this region may be due to the local minima created by noisy aerodynamic response and to the lack of derivative information for the interlacing factor. The interlacing factors remained less than 1 in the third case, but unfortunately the aerodynamic optimizer could not find a way to escape the local minimum.

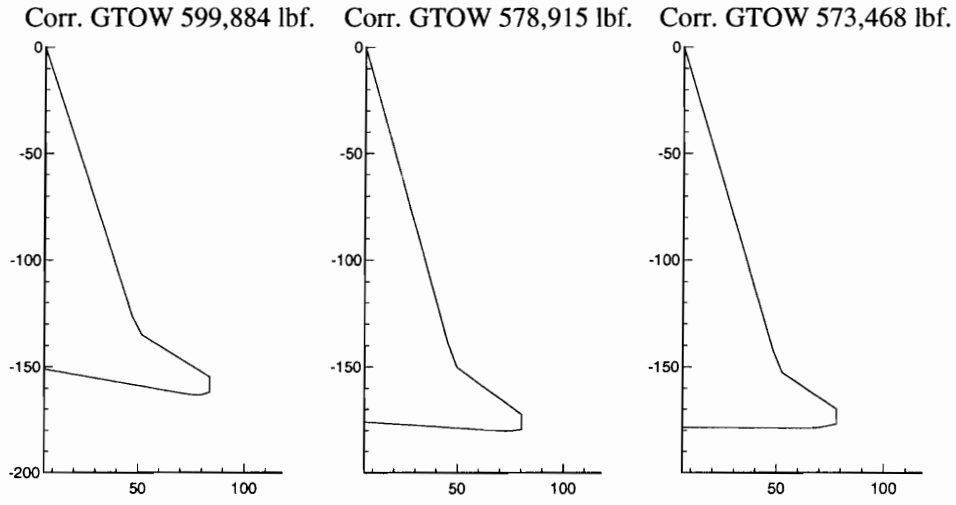

Figure 4.4 Planforms, Case 1 (All dimensions in ft.).

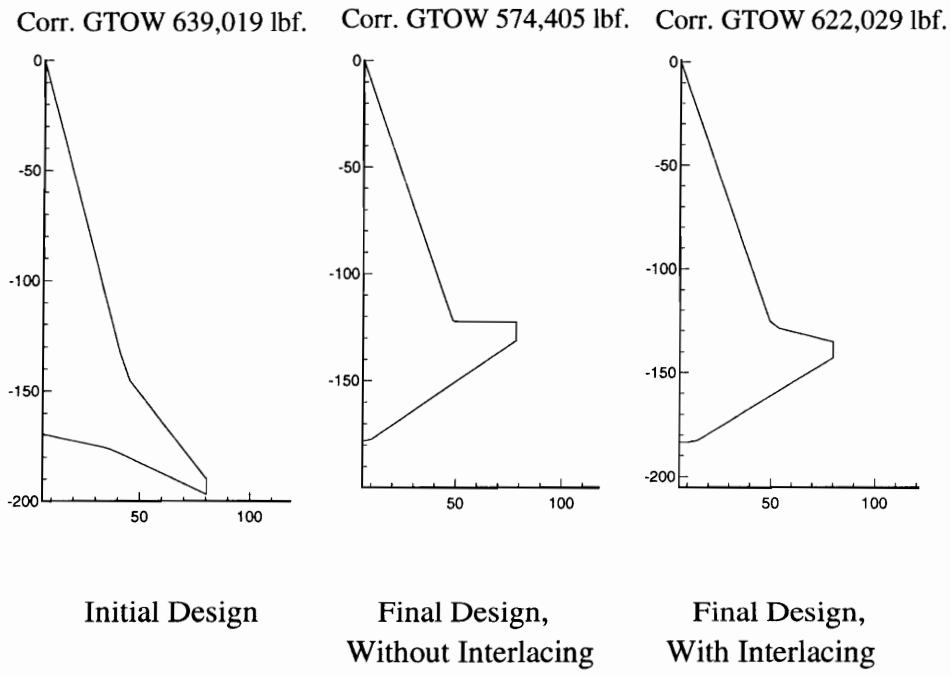

Figure 4.5 Planforms, Case 2 (All dimensions in ft.).

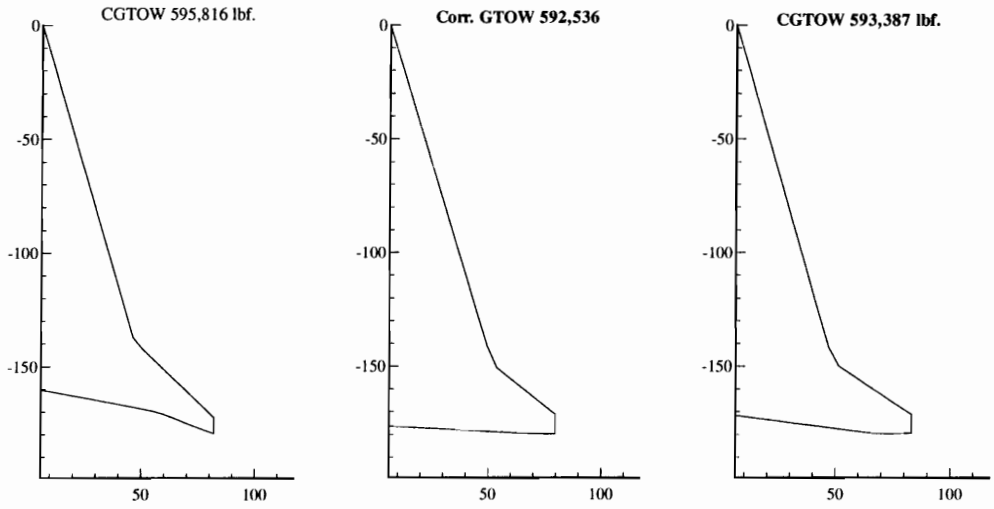

Figure 4.6 Planforms, Case 3 (All dimensions in ft.).

Table 4.2. Selected Design Parameters, Case 1.

	starting design	opt. design without interlacing	opt. design with interlacing
GTOW *, lbf.	599884	578915	573468
fuel weight *, lbf.	299900	280274	271980
wing weight, lbf.	97363	97123	98821
fuselage weight, lbf.	37449	36187	36927
wing area, ft^2	10767	12141	12511
AR	2.60	2.12	2.25
span, ft	167.3	160.5	156.7
inboard LE sweep angle	71.98	74.18	73.25
inboard TE sweep angle	9.94	3.71	0.307
outboard LE sweep angle	31.56	35.93	32.58
outboard TE sweep angle	-17.22	-10.32	-13.86
root t/c, %	2.58	2.56	2.25
break t/c, %	2.23	2.27	1.85
tip t/c, %	1.94	2.55	2.01
(L/D)max	10.01	9.99	10.35
landing angle	12.38	11.92	11.99
interlacing factor	1.010	0.972	0.998

* corrected for range deficiency

Table 4.3. Selected Design Parameters, Case 2.

	starting design	opt. design without interlacing	opt. design with interlacing
GTOW *, lbf.	639019	574405	622029
fuel weight *, lbf.	320947	285844	310907
wing weight, lbf.	110881	89411	105959
fuselage weight, lbf.	40263	34811	37716
wing area, ft^2	11460	12247	13252
AR	2.52	2.00	1.92
span, ft	160.7	156.5	159.6
inboard LE sweep angle	75.25	70.83	70.92
inboard TE sweep angle	51.79	65.18	0.046
outboard LE sweep angle	12.22	0.004	13.66
outboard TE sweep angle	25.33	-34.03	-31.33
root t/c, %	2.14	2.30	2.83
break t/c, %	1.73	2.07	2.22
tip t/c, %	1.51	2.19	2.16
(L/D)max	11.10	9.74	9.83
landing angle	12.58	11.92	12.00
interlacing factor	1.169	1.391	1.501

* corrected for range deficiency

Table 4.4. Selected Design Parameters, Case 3.

	starting design	opt. design without interlacing	opt. design with interlacing
GTOW *, lbf.	595861	592536	593387
fuel weight *, lbf.	293045	289079	291567
wing weight, lbf.	99574	100759	99428
fuselage weight, lbf.	37880	36559	36632
wing area, ft^2	10988	12754	12073
AR	2.45	2.00	2.29
span, ft	164.0	159.6	166.1
inboard LE sweep angle	73.66	78.89	73.94
inboard TE sweep angle	10.62	3.01	7.27
outboard LE sweep angle	43.64	38.49	33.82
outboard TE sweep angle	21.10	-2.27	-1.79
root t/c, %	2.36	2.62	2.71
break t/c, %	1.98	2.19	2.25
tip t/c, %	1.72	2.15	2.38
(L/D)max	10.63	10.14	10.04
landing angle	12.47	11.87	11.81
interlacing factor	0.969	0.896	1.004

* corrected for range deficiency

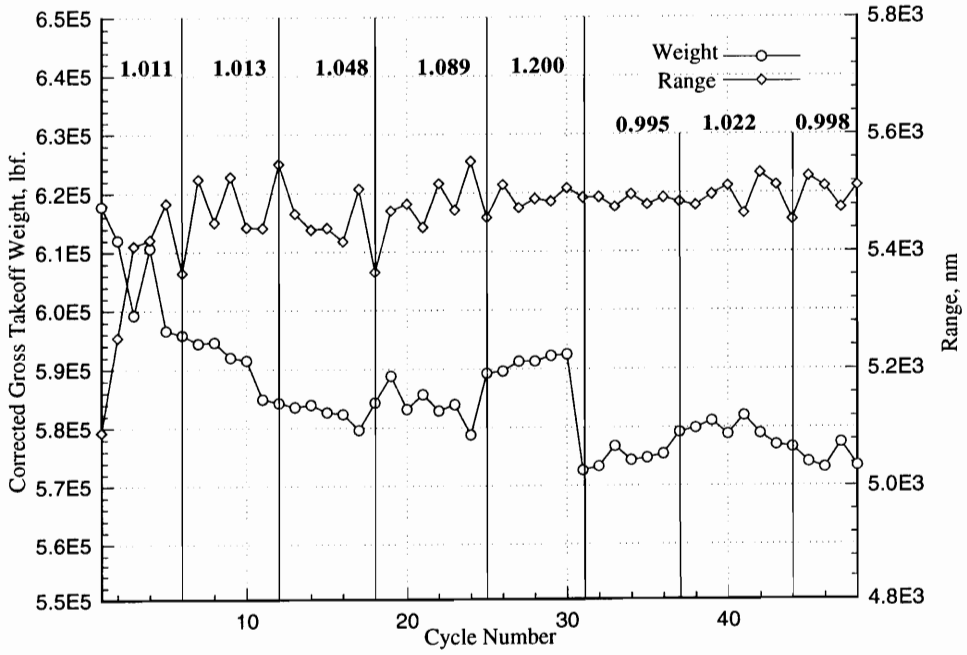

Figure 4.7 Convergence History of GTOW and Range, Case 1.

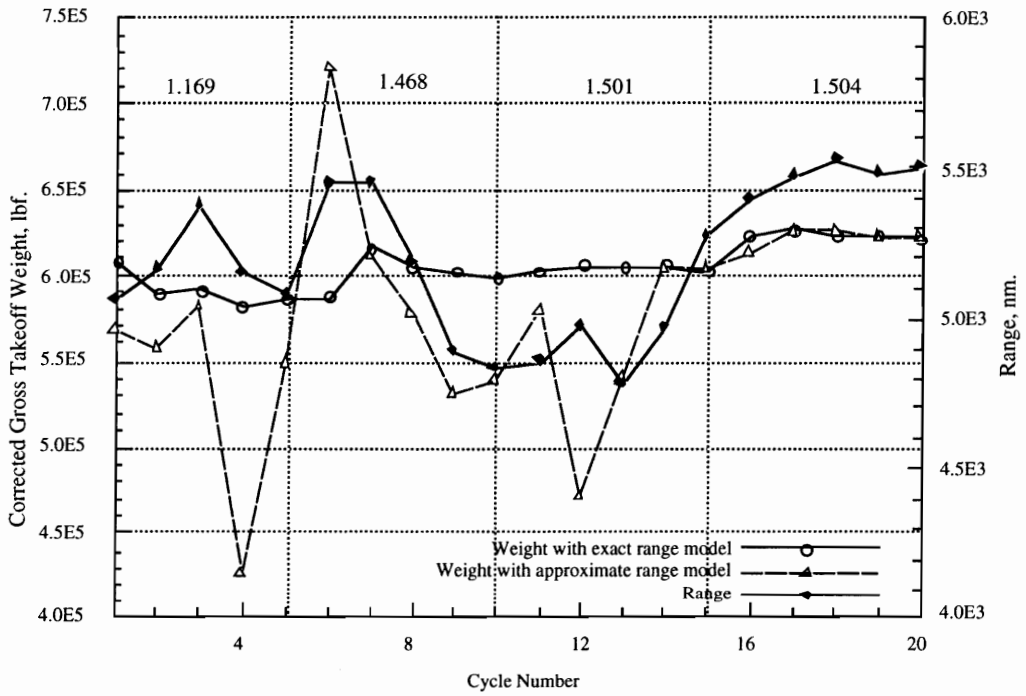

Figure 4.8 Convergence History of GTOW and Range, Case 2.

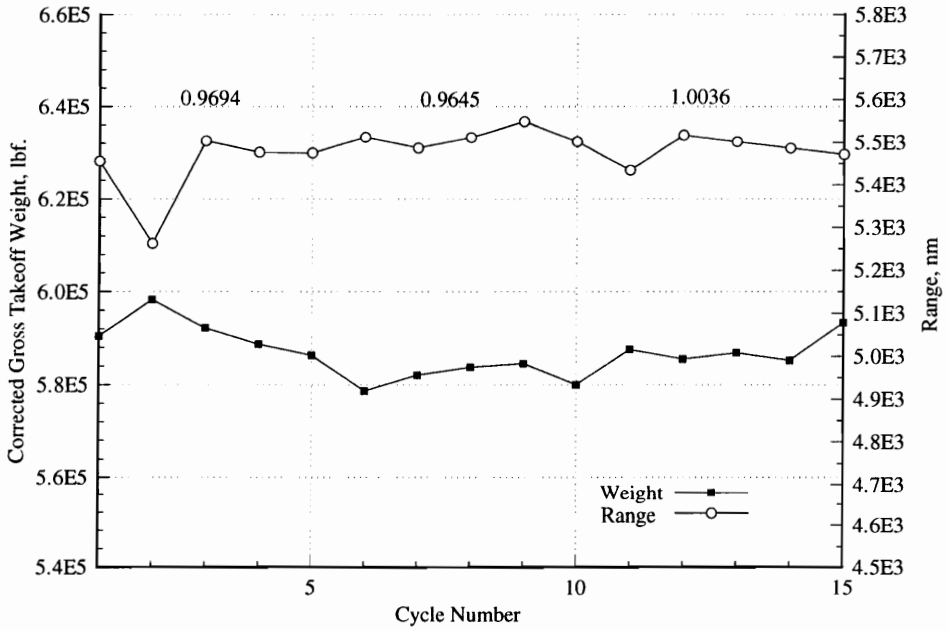

Figure 4.9 Convergence History of GTOW and Range, Case 3.

5. Conclusions

A finite-element-model based structural optimization procedure was successfully implemented to provide accurate estimation of wing bending material. Static aeroelastic effects were considered using a flexible load evaluation procedure developed for this study. Several designs were optimized for both rigid and flexible loads under several flight conditions. The detailed comparison of the results based on rigid and flexible loads showed that static aeroelastic effects were small for most high speed civil transport designs we discussed and structural optimization based on rigid loads can be considered as a conservative weight estimation procedure. The results of the structural optimization were compared with estimates from two algebraic weight equations. The comparison indicates that the simple weight equations are good at predicting the average structural weight and effects of wing thickness on structural weight, but may not model accurately all the effects of planform changes on the structural weight. Even though the Grumman weight equation is more detailed than the FLOPS weight equation, the FLOPS weight equation agrees much better with structural optimization than the Grumman weight equation.

We have developed a strategy of interlacing aerodynamic and structural optimization in the design of the high-speed civil transport. This strategy uses the result of a full structural optimization, performed periodically, to scale the wing weight estimated by the FLOPS weight equation. Three studies were performed, each with a design which was optimized with and without the interlacing procedure. The results indicate that the interlacing procedure was able to prevent the optimizer from obtaining designs based on optimistic weight equations. However, because of noisy aerodynamic response and possibly because of lack of derivatives of

the interlacing factor, the optimizer could not extricate itself from regions in design space corresponding to poor designs.

Future work in this area will involve the implementation of three levels of complexity for the structural analysis, utilizing the weight equation and both simple and refined finite-element models. The derivatives of the interlacing scale factors should be used to let the aerodynamic optimizer escape the invalid domains where the weight equation is inaccurate. The smooth approximation of aerodynamic responses and the response surface fit of wing bending material based on structural optimization results will also be used to escape the local mimima.

REFERENCES

1. Haftka, R. T., "Optimization of Flexible Wing Structures Subject to Strength and Induced Drag Constraints", AIAA Journal, Vol. 14, No. 8, pp. 1101-1106, 1977.
2. Shirk, M. H., Hertz, T. J. and Weisshaar, T. A., "Aeroelastic Tailoring-Theory, Practice, and Promise", Journal of Aircraft, Vol. 23, No. 1, pp. 6-18, 1986.
3. Haftka, R. T., "Structural Optimization with Aeroelastic Constraints - A Survey of US Applications", International Journal of Vehicle Design", Vol. 7, No. 3 & 4 , pp. 381-392, 1986.
4. Malone, B., and Mason, W. H., "Multidisciplinary Optimization in Aircraft Design Using Analytic Technology Models", AIAA Paper 91-3187, 1991.
5. Malone, B., and Mason, W. H., "Aircraft Concept Optimization in Aircraft Design using Approach and Parametric Multiobjective Figures of Merit ", AIAA Paper 92-4221,1992.
6. Gogate, S., Pant, R., and Arora, P., "Incorporation of Some Cost and Economic Parameters in the Conceptual Design Optimization of an Air-Taxi Aircraft", AIAA Paper 94-4301, 1994.
7. McGeer, T., "Wing Design for Minimum Drag with Practical Constraints", Journal of Aircraft, Vol. 21, No. 11, pp. 879-920, 1984 .
8. Grossman, B., Haftka, R. T., Kao, P.-J., Polen, D. M., Rais-Rohani, M., and Sobieszczanski-Sobieski, J., "Integrated Aerodynamic-Structural Design of a Transport Wing", Journal of Aircraft, Vol. 27, No. 12, pp. 1050-1056, 1990.
9. Wakayama, and Kroo, "A Method for Lifting Surface Design using Nonlinear Optimization", AIAA Paper 90-3290, 1990.

10. Gallman, J. W., Kroo, I. M., and Smith, S. C., "Design Synthesis and Optimization of Joined-Wing Transports", AIAA Paper 90-3197, 1990.

11. Gallman, J. W., Kaul, R. W., Chandrasekaran, R. M., and Hinson, M. L., "Optimization of an Advanced Business Jet", AIAA Paper 94-4304, 1994.

12. McCullers, L. A., "Aircraft Configuration Optimization Including Optimized Flight Profiles", Proceedings of a Symposium on Recent Experiences in Multidisciplinary Analysis and Optimization, J. Sobieski, compiler, NASA CP-2327, pp. 395-412, 1984.

13. Vanderplaats, G., "Automated Optimization Techniques for Aircraft Synthesis", AIAA Paper 76-909, 1976.

14. Mason, W. H., and Arledge, T. K., "ACYNT Aerodynamic Estimation - AN Examination and Validation for Use in Conceptual Design", AIAA Paper 93-0973, 1993.

15. Stubbe, J. R., "PASCOS - A Multidisciplinary Design Optimization Tool for Hypersonic Vehicle Design", AIAA Paper 92-4723, 1992.

16. Daum, A., and Wolf, D., "TRANSYS - A Multidisciplinary Optimization Software System for Preliminary Design, Analysis, and Evaluation of Space Transportation Systems", AIAA Paper 94-4342, 1994.

17. Rais-Rohani, M., Haftka, R. T., Grossman, B., and Unger, E. R., "Integrated Aerodynamic-Structural-Control Wing Design", AIAA Paper 92-4694, 1992.

18. Unger, E. R., Hutchison, M. G., Rais-Rohani, M., Haftka, R. T., and Grossman, B., "Variable Complexity Interdisciplinary Design of a Transport Wing", International Journal of Systems Automation Research and Application, Vol. 2, No. 2, pp. 87-113, 1992.

19. Barthelemy, J.-F. M., Wrenn, G. A., Dovi A. R., Coen, P. G., and Hall, L. E., "Supersonic Transport Wing Minimum Weight Design Integrating Aerodynamics and Structures", Journal of Aircraft, Vol. 31, No. 2, pp. 330-338, 1994.

20. Tzong, G., Baker, M., Yalamanchili, K., and Giesing, J., "Aeroelastic Loads and Structural Optimization of a High Speed Civil Transport Model", AIAA Paper: 94-4378, 1994.

21. Wakayama, S., and Kroo, I., "Subsonic Wing Design Using Multidisciplinary Optimization", AIAA Paper: 94-4409, 1994.

22. Brugeen, G. W., and Baysal, O., "Three-Dimensional Aerodynamic Shape Optimization of Supersonic Delta Wings", AIAA Paper: 94-4271, 1994.

23. Welge, R. H., "Aerodynamic Technology Opportunities for a High-Speed Civil Transport", SAE Paper 881354., 1988.

24. Chang, I. C., and Torres, F. J., "Wing Design Code Using Three-Dimensional Euler Equations and Optimization", AIAA Paper: 91-3190, 1991.

25. Korivi, V., Taylor, A., and Newman, P., "Aerodynamic Optimization Studies Using 3-D Supersonic Euler Code with Efficient Calculation of Sensitivity Derivatives", AIAA Paper: 94-4270, 1994.

26. Sobieszczanski-Sobieski, J., "Sensitivity Analysis and Multidisciplinary Optimization for Aircraft Design: Recent Advances and Results", I.C.A.S., Paper 88-1.7.3, 1988

27. Sobieszczanski-Sobieski, J., "On the Sensitivity of Complex Internally Coupled Systems", AIAA Paper CP-8-2378, and AIAA Journal, Vol. 28, No. 1, 1990.

28. Balling, R., and Sobieszczanski-Sobieski, J., "An Algorithm for Solving the System-Level Problem in Multilevel Optimization", AIAA Paper 94-4333, 1994

29. Wrenn, G. A., and Dovi, A. R., "Multilevel Decomposition Approach to the Preliminary Sizing of a Transport Aircraft Wing", Journal of Aircraft, Vol. 25, No. 7, pp. 632-638, 1988

30. Röhl, P., and Schrage, D., "Preliminary Wing Design of a High Speed Civil Transport Aircraft by Multilevel Decomposition Techniques", AIAA Paper AIAA Paper 92-4841, 1992.

31. Eason, E., Nystrom, G., Burlingham A. and Nelson, E., "Non-Hierarch Multidisciplinary Design of a Commercial Aircraft", AIAA Paper 94-4302, 1994.

32. Kulfan, R. M., "Application of Favorable Aerodynamic Interference to Supersonic Airplane Design", SAE Paper 901988, 1990.

33. Borland, C. J., Benton, J. R., Frank, P. D., Kao, T. J., Mastro, R. A., and Barthelemy, J-F. M., "Multidisciplinary Design Optimization of a Commercial Aircraft Wing - An Exploratory Study", AIAA Paper 94-4305, 1994.

34. Hutchison, M. G., Unger, E. R., Mason, W., Grossman, B., and Haftka, R. T., "Variable Complexity Aerodynamic Optimization of a High-Speed Civil Transport Wing", Journal of Aircraft, Vol. 31, No. 1, pp. 110-116, 1994.

35. Hutchison, M. G., "Multidisciplinary Optimization of High-Speed Civil Transport Configurations using Variable-Complexity Modeling ", Ph.D. Dissertation, Virginia Polytechnic Institute and State University, 1993.

36. Hutchison, M. G., Huang, X., Mason, W. H., Haftka, R. T., and Grossman, B., "Variable-Complexity Aerodynamic-Structural Design of a High-Speed Civil Transport Wing", AIAA Paper 92-4695, 1992.

37. Huang, X., Haftka, R. T., Grossman, B., and Mason, W. H., "Comparison of Statistical Weight Equations with Structural Optimization for Supersonic Transport Wings", AIAA Paper 94-4379, 1994.

38. Dudley, J., Huang, X., Haftka, R. T., Grossman, B., and Mason, W. H., "Variable-Complexity Interlacing of Weight Equation and Structural Optimization for the Design of the High-Speed Civil Transport", AIAA Paper 94-4377, 1994.

39. Coen, P. G., Sobieszczanski-Sobieski, J., and Dollyhigh, S. M., "Preliminary Results from the High-Speed Airframe Integration Research Project", AIAA Paper 92-1004, 1992.

40. Craidon, C. B., "Description of a Digital Computer Program for Airplane Configuration Plots", NASA TM X-2074, 1970.

41. Grandhi, R. V., Thareja, R. and Haftka, R. T., "NEWSUMT-A: A General Purpose Program for Constrained Optimization using Constraint Approximations", ASME Journal of Mechanisms, Transmissions and Automation in Design, 107, pp. 94-99, 1985.

42. D'Vari, R., Baker, M., "A Static and Dynamic Aeroelastic Loads and Sensitivity Analysis For Structural Loads Optimization and Its Application to Transport Aircraft", AIAA Paper 93-1643, 1993.

43. Cruz, J., "Efficient Calculation of Aeroelastic Loads and Sensitivities", private communication, 1992.

44. Margason, R. J., and Lalmar, J. E., "Vortex-Lattice FORTRAN Program for Estimating Subsonic Aerodynamic Characteristics of Complex Planforms", NASA TN D-6142, 1977.

45. Bertin, J. J., and Smith, M. L., "Aerodynamics for Engineers", 2nd Edition, Prentice Hall, 1989.

46. Carlson, H. W., and Miller, D S., " Numerical Methods for the Design and Analysis of Wings at Supersonic Speeds", NASA TN D-7713, 1974.

47. Carlson, H. W., and Mack, R. J., " Estimation of Leading-Edge Thrust for Supersonic Wings of Arbitrary Planforms", NASA TP-1270, 1978.

48. Harder, R. L., and Desmarais, R. N., "Interpolation using Surface Spline", Journal of Aircraft, Vol. 9, No. 2, pp. 189-191, 1972.

49. Press, W. H., Flannery, B. P., Tukolsky, S. A., and Vetterling, W. T., "Numerical Recipes, The Art of Scientific Computing", Combridge University Press, 1986.

50. Whestone, W. D., "Engineering Analysis Language Reference Manual", Engineering Information System, Incorporated, 1983.

51. Young, W. C., " Roak's Formulas for Stress and Strain ", 6th Edition, McGraw-Hill Book Company, 1988.

52. Torenbeek, E., "Development and Application of a Comprehensive, Design-sensitive Weight Prediction Method for Wing Structures of Transport Category Aircraft", Report LR-693, Delft University of Technology, 1992.

53. Scott, P. W, "Developing Highly Accurate Empirical Weight Estimating Relationships: Obstacles and Tactics", Proceedings of 51th International Conference of the Society of Weight Engineers, SAWE Paper No. 2091, 1992.

54. York, P., and Labell, R., "Aircraft Wing Weight Build-Up Methodology with Modification for Materials and Construction Techniques", NASA CR-166173, 1980.

55. Shields, E. W., McCullers, L. A., "Development of a Weight Equation for Unconventional Transport Aircraft Wings", Memorandum, File: 3-92000/4LTR-091, 1984.

56. Unger, E., and Hall, L., "The Use of Automatic Differentiation in an Aircraft Design Problem", AIAA Paper 94-4260, 1994.

57. Giunta, A., Dudley, J., Grossman, B., Haftka, R. T., Mason, W., and Watson, L., "Noisy Aerodynamic Response and Smooth Approximations in HSCT Design", AIAA Paper 94-4376, 1994.

VITA

The author was born in Changsha, China on February 12, 1964. He completed his elementary and secondary education in Changsha, and received his High School Diploma from Mingda high school in 1981. He got his B. S. degree in Engineering Mechanics from Huazhong University of Science and Technology in 1985. In 1988, he graduated from Dalian University of Technology with a Master degree in Engineering Mechanics, and then joined Beijing Central Engineering Research Institute for Non-ferrous Metallurgical Industries.

In pursuit of higher education he came to the United States in January 1991, and studied in University of Miami for a semester. In summer of 1991, he was accepted to the Ph.D. program in Aerospace Engineering at Virginia Polytechnic Institute and State University.

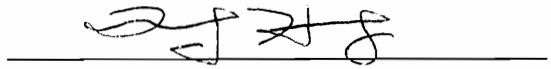

Ximing Huang